

Report

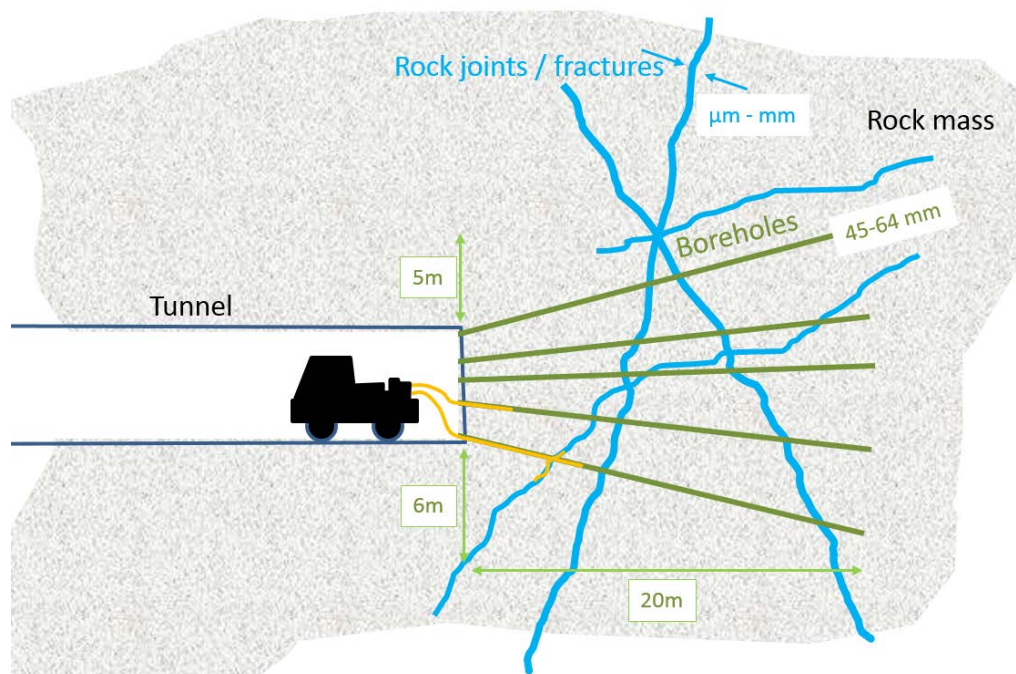
NUMERICAL SIMULATIONS OF GROUT FLOW IN SIMPLIFIED GEOMETRIES

Subtitle

Author(s)

Sjur Mo

Paal Skjetne



Report

NUMERICAL SIMULATIONS OF GROUT FLOW IN SIMPLIFIED GEOMETRIES

Enterprise /VAT No:
NO 948 007 029 MVA**KEYWORDS:**Grout flow
Grouting
CFD
numerical modelling
rheology**Subtitle****VERSION**

7

DATE

2017-04-21

AUTHOR(S)Paal Skjetne
Sjur Mo**CLIENT(S)**

TIGHT

CLIENT'S REF.

Eivind Grøv

PROJECT NO.

102009275-4

NUMBER OF PAGES/APPENDICES:

40 + 0 Appendices

ABSTRACT**Abstract heading**


In this work, we demonstrate how computational fluid dynamics (CFD) can contribute to improved understanding of the basics of grout flow. As a starting point, we have limited the scope to a simplified geometry consisting of a single borehole crossing a joint, but this can easily be extended to more complex geometries. We start by presenting some simplified analytical results before we turn to the CFD simulations. The simulations showed (as expected) that viscous effects dominate, meaning that joint orientation does not influence inflow from the bore hole. However, the exposure area of the joint to the borehole increases for decreasing angle (borehole and joint becoming more parallel) improving the inflow. This means that simplified models such as axis-symmetric models and in particular models of only the joint (3D) with an ellipsoidal inlet in many cases will give sufficiently accurate estimates. The simulations indicated that grout injectivity seems to be enhanced by a residual water film on the walls near the grout front. Furthermore, we show how rheology of cement-based grouts influences the flow in the above examples. Rheology parameters are varied within typical ranges for cement-based grouts to map the model sensitivity to these parameters.

PREPARED BY

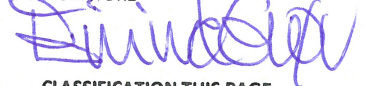
Paal Skjetne

SIGNATURE**CHECKED BY**

John C. Morud

SIGNATURE**APPROVED BY**

Eivind Grøv

SIGNATURE**REPORT NO.**

SINTEF A28153

ISBN

978-82-14-06068-3

CLASSIFICATION

Unrestricted

CLASSIFICATION THIS PAGE

Unrestricted

Document history

VERSION	DATE	VERSION DESCRIPTION
7	2017-04-21	Converted from Memo: " TIGHT: Numerical simulations of cement injection" version 6c.

Table of contents

1	INTRODUCTION	5
2	CEMENT PROPERTIES.....	6
2.1	Density	6
2.2	Viscosity - Marsh cone test	6
2.3	Default values	7
3	SIMPLE ESTIMATES	7
3.1	Typical velocities	7
4	SIMPLIFIED MODELS	8
4.1	2D Models	8
4.2	Axial symmetry (radial flow) in a single joint.....	8
4.2.1	Spatially varying joint aperture	9
4.3	Pipe flow	11
4.4	Pressure drop in bends	11
4.5	Non-Newtonian fluids.....	12
4.5.1	Herschel-Bulkley fluid	13
4.5.1.1	Pipe flow of Herschel-Bulkley fluid.....	13
4.5.1.2	Channel flow of Herschel-Bulkley fluid.....	13
4.6	Joint spacing etc.....	16
5	ANSYS FLUENT SIMULATIONS	18
5.1	Single phase tests.....	18
5.1.1	Fully 3D simulations.....	19
5.1.1.1	Effect of joint angle in simulation with both borehole and joint resolved.....	19
5.1.1.2	Effect of joint angle when simplifying to joint only being resolved	20
5.1.2	Reduced dimensionality – 2D	24
5.1.2.1	Joint angle.....	24
5.1.3	Axis symmetric 3D model	25
5.1.3.1	Joint angle.....	25
5.1.3.2	Joint aperture	26
5.1.3.3	Joint aperture variations – Porous zone.....	26
5.1.4	Full 3D model of joint:	29
5.1.4.1	Joint aperture variations – Modified geometry	31
5.1.4.2	Joint aperture variations – Ensemble averaging	32
5.1.5	Non-Newtonian single phase fluid	32

5.2	Cement replacing water (2-phase, Fluent)	33
5.2.1	3D Axis symmetric – Newtonian.....	33
5.2.1.1	Joint angle.....	33
5.2.2	3D Axis symmetric - Non-Newtonian.....	35
5.2.2.1	Yield stress effect.....	35
6	SUMMARY	38
7	FUTURE WORK	38
8	SYMBOL LIST	39
9	REFERENCES	40

APPENDICES

NONE

1 INTRODUCTION

The objective of this work package in the TIGHT¹ project is to investigate how flow modelling can contribute to improve understanding of the flow mechanisms related to tunnel grouting. Focusing on a single borehole the situation is as sketched in Figure 1. A number of such holes are drilled around the rock face to be excavated and the fracture network or joint network between neighbouring holes are connected. In this report we limit the scope to flow from a single borehole into its adjoining joint network. In particular we look at how the grout flows from the borehole into the joint network. The current target for operations is to have approx. 5 m plugging, i.e. the grout shall preferably flow at least 5 m into the joints and when set block the whole aperture (to avoid leakage).

We start by some simple estimates for the cement properties before we present different simplified analytical models that were of helpful in guiding the simulation work. Some of these results may also be useful tools to get quick estimates. Then we proceed to the CFD simulations using ANSYS Fluent. Finally, we summarize and outline suggestions for further work.

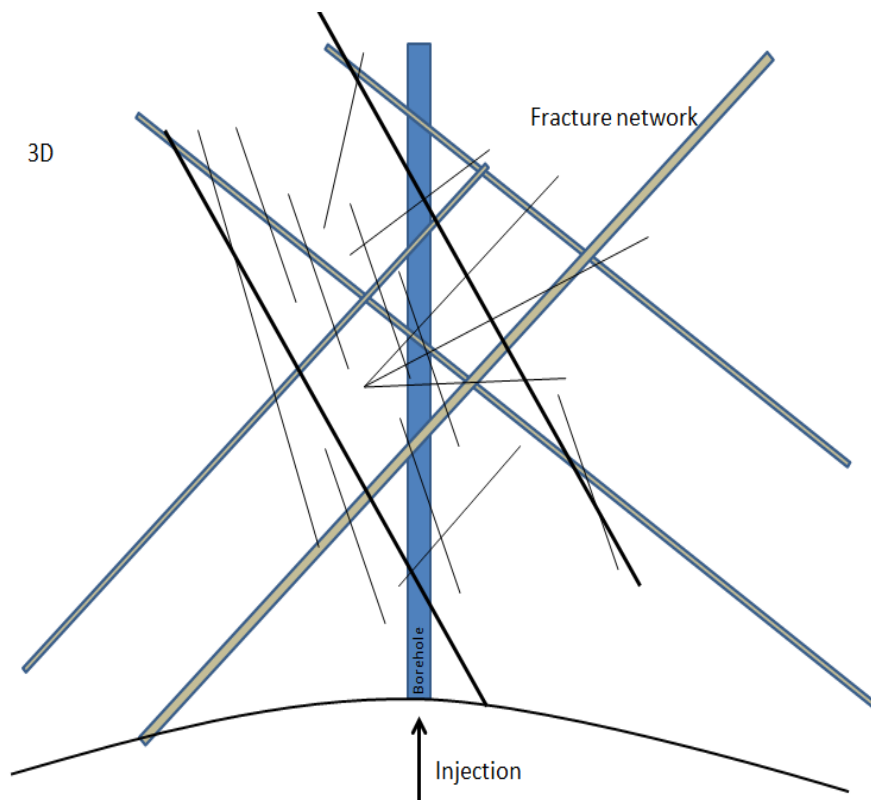


Figure 1: Borehole with fracture/joint network.

¹ True Improvement in Grouting High pressure technology for Tunnelling (TIGHT)

2 CEMENT PROPERTIES

The most important cement properties are density, viscosity (rheology) and grain size. In the current simulations, the cement is treated as a single fluid phase with given density and viscosity (rheology). This means that grain size only influences rheology. Later this approach can be extended to study cements as being composed of water and solid particles. The latter approach will allow studying bleeding effects etc.

2.1 Density

The water/cement ratio is given by the mass ratio:

$$\xi_{w/c} = \frac{m_w}{m_c} \quad (0.1)$$

The mixture density is then:

$$\rho_{c,mix} = \frac{\rho_w V_w + \rho_c V_c}{V_w + V_c} = \frac{m_w + m_c}{m_w/\rho_w + m_c/\rho_c} = \frac{1 + \xi_{w/c}}{1 + \frac{\rho_c}{\rho_w} \xi_{w/c}} \rho_c \quad (0.2)$$

See Figure 2 for some examples.

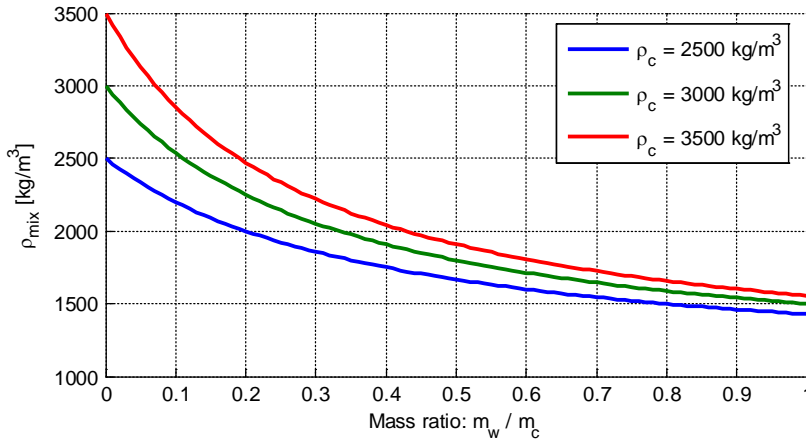


Figure 2: Mixture density as function of mass ratio for different cement densities for $\rho_w = 1000 \text{ kg/m}^3$.

2.2 Viscosity - Marsh cone test

For a Marsh cone with $d = 4.76 \text{ mm}$ orifice diameter the effective viscosity (in cP) can be estimated by the following correlation [3]:

$$\mu_{c,mix}(t_{empty}; \rho_{c,mix}) = \exp \left[\left(\ln \left(\frac{t_{empty} - 24.5}{0.58} \right) / 1.2 \right) + \ln \left(\frac{\rho_{c,mix}}{1000} \right) \right] \quad (0.3)$$

where t_{empty} is the measured emptying time (in seconds) and $\rho_{c,mix}$ is the mixture density in kg/m^3 . It seems that this can be simplified to:

$$\mu_{c,mix}(t_{empty}; \rho_{c,mix}) \approx 0.001575 \rho_{c,mix} (t_{empty} - 24.5)^{0.833} \quad (0.4)$$

See Figure 3 for some examples.

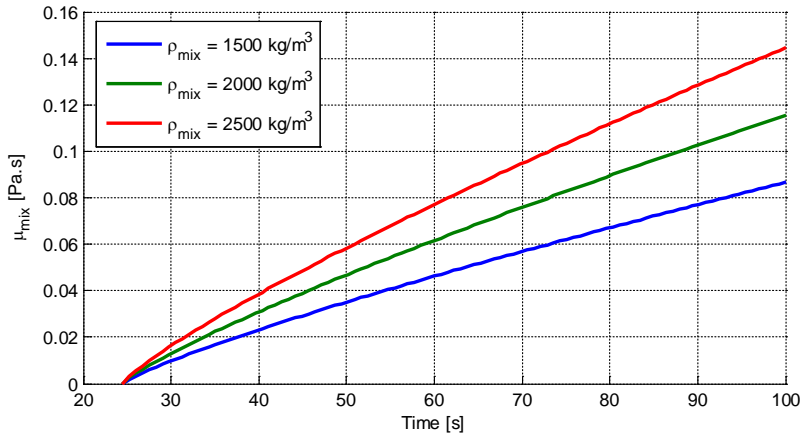


Figure 3: Viscosity from Marsh-cone test.

2.3 Default values

In this report, we have used the following values:

$$\begin{aligned} \rho_{c,mix} &= 1600 \text{ kgm}^{-3}, & \mu_{c,mix} &= 0.050 \text{ Pa} \cdot \text{s} \\ \rho_w &= 1000 \text{ kgm}^{-3}, & \mu_w &= 0.001 \text{ Pa} \cdot \text{s} \end{aligned} \quad (0.5)$$

if not specifically specified differently.

3 SIMPLE ESTIMATES

3.1 Typical velocities

A maximal inlet flow rate of $Q = 30$ liter/min is a typical limit [1]. For a borehole with diameter $D_b = 54$ mm this corresponds to:

$$U_{in} = \frac{Q}{\pi (D_b/2)^2} = \frac{Q}{\pi R_b^2} \approx 0.22 \text{ m/s} \quad (0.6)$$

and we have introduced the borehole radius $R_b = D_b/2$. For a single axisymmetric joint with aperture h oriented normal to the borehole direction the radial flow velocity in the joint decreases with radius as:

$$U_{joint}(r) = \frac{Q}{2\pi r h} = U_{joint}^{in} \frac{R_b}{r}, \quad (0.7)$$

where:

$$U_{joint}^{in} = U_{joint}(R_b) = \frac{Q}{2\pi R_b h} = \frac{2.94 \text{ mm}}{h} \text{ m/s} \quad (0.8)$$

is the velocity in the joint inlet for a flow rate into the borehole of 30 liter/min and only a single joint along the borehole.

4 SIMPLIFIED MODELS

It is useful to study simplified models to get some ideas about expected behaviour before embarking on heavy simulations.

4.1 2D Models

The pressure gradient between two smooth parallel plates in the laminar flow regime is given by:

$$\frac{dp}{dx} = -\frac{12\mu Q}{h^3 w} = -\frac{12\mu U_{in}}{h^2} \quad (0.9)$$

where the cross-sectional area is $A = hw$. Roughness effects are accounted for by including an additional factor [2]:

$$f_\varepsilon = 1 + 3.1 \left(\frac{\varepsilon}{h} \right)^{1.5} \quad (0.10)$$

such that:

$$\frac{dp}{dx} = -f_\varepsilon \frac{12\mu Q}{h^3 w} = -f_\varepsilon \frac{12\mu U_{in}}{h^2} \quad (0.11)$$

4.2 Axial symmetry (radial flow) in a single joint

From mass balance the front propagation velocity in a joint is (assuming sharp front / plug flow):

$$\frac{dr}{dt} = \frac{Q}{2\pi h r} = \frac{U_{in} \pi R_b^2}{2\pi h} \frac{1}{r} = \frac{R_b^2 U_{in}}{2h} \frac{1}{r} \quad (0.12)$$

and the total time to fill the joint out to a radius r_{joint} is:

$$t(r_{joint}) = \frac{\pi r_{joint}^2 h}{Q} = \frac{h}{U_{in}} \left(\frac{r_{joint}}{R_b} \right)^2 \quad (0.13)$$

The pressure profile can be approximated as [1]:

$$\begin{aligned} p(r) - p(R_b) &= -f_\varepsilon \frac{12\mu Q}{2\pi h^3} \ln\left(\frac{r}{R_b}\right) + \frac{3\rho Q^2}{20\pi^2 h^2} \left[\frac{1}{R_b^2} - \frac{1}{r^2} \right], \quad Q = 2\pi h R_b U_{joint}^{in} \\ &= \underbrace{-f_\varepsilon \frac{12\mu U_{joint}^{in}}{h^2} R_b \ln\left(\frac{r}{R_b}\right)}_{\text{Viscous}} + \underbrace{\frac{3\rho (U_{joint}^{in})^2}{5} \left[1 - \left(\frac{R_b}{r}\right)^2 \right]}_{\text{Inertial}} \end{aligned} \quad (0.14)$$

where the first term is the viscous pressure drop and the second is the inertial pressure change due to fluid deceleration in the radial direction (Bernoulli effect).

The viscous term is dominant when:

$$\frac{12\mu Q}{2\pi h^3} \ln\left(\frac{r}{R_b}\right) \gg \frac{3\rho Q^2}{20\pi^2 h^2} \left[\frac{1}{R_b^2} - \frac{1}{r^2} \right] \quad (0.15)$$

By introducing δ as the distance into the joint (from $r = R_b$), i.e. $r = R_b + \delta$ this can be written as:

$$\frac{40\pi\mu R_b^2}{\rho Q h} \ln(1+x) \gg \left[1 - (1+x)^{-2} \right], \quad x = \frac{\delta}{R_b} \quad (0.16)$$

The terms are equal when:

$$f(x) = \frac{\xi}{h} - \frac{1 - (1+x)^{-2}}{\ln(1+x)} = 0, \quad \xi = \frac{40\pi\mu R_b^2}{\rho Q} \quad (0.17)$$

The solution is shown in Figure 4 (in our case $\xi \approx 0.11$ m). There is no solution for $h < 1.4$ mm showing that for such small apertures the viscous term is always larger than the inertial term. For larger apertures it gives the number of borehole diameters into the joint for which deceleration effects are comparable to the viscous effects.

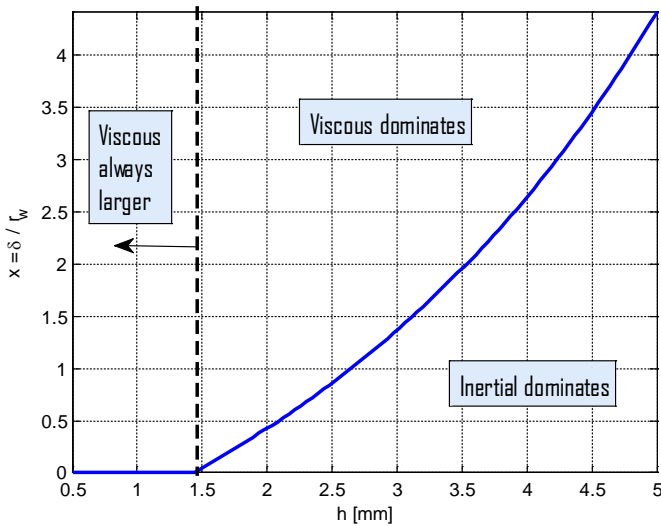


Figure 4: Solution of Eq. (1.17).

It is also useful to calculate the pressure gradient from Eq. (1.14):

$$\frac{dp}{dr} = -f_\varepsilon \frac{6\mu Q}{\pi h^3} \frac{1}{r} + \frac{3\rho Q^2}{10\pi^2 h^2} \frac{1}{r^3} \quad (0.18)$$

4.2.1 Spatially varying joint aperture

For a radially varying aperture $h = h(r)$ we get (when neglecting the inertial term):

$$\Delta p[h] = p(r) - p_w = -f_\varepsilon \frac{6\mu Q}{\pi} \int_{R_b}^r dr \frac{1}{rh^3(r)} \quad (0.19)$$

Example:

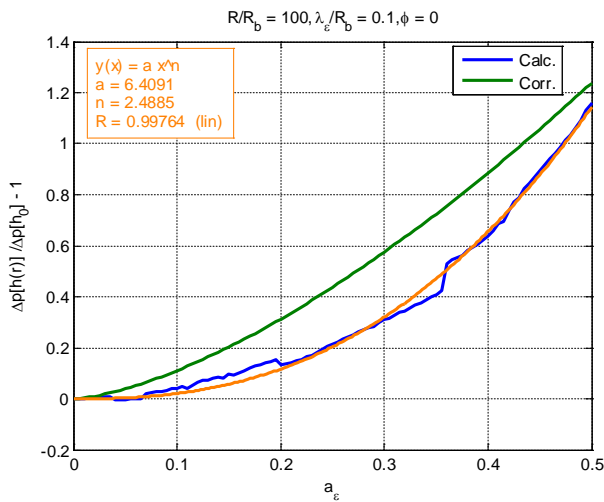
$$h(r) = h_0 \left\{ 1 + a_\varepsilon \sin \left[2\pi (r - R_b) / \lambda_\varepsilon \right] \right\} \quad (0.20)$$

Then:

$$\frac{\Delta p[h]}{\Delta p[h_0]} = \frac{\int_{R_b}^r \frac{dr}{rh^3(r)}}{\int_{R_b}^r \frac{dr}{rh_0^3}} = \frac{\int_{R_b}^r \frac{dr}{r \left\{1 + a_\varepsilon \sin \left[\frac{2\pi(r - R_b)}{\lambda_\varepsilon} \right] \right\}^3}}{\ln \left(\frac{r}{R_b} \right)} \quad (0.21)$$

By using a small 'wave-length' we can emulate roughness effects. An example is shown in Figure 5. It seems that the correlation in Eq. (1.10) may give a high estimate of roughness effects.

Radial:



1D:

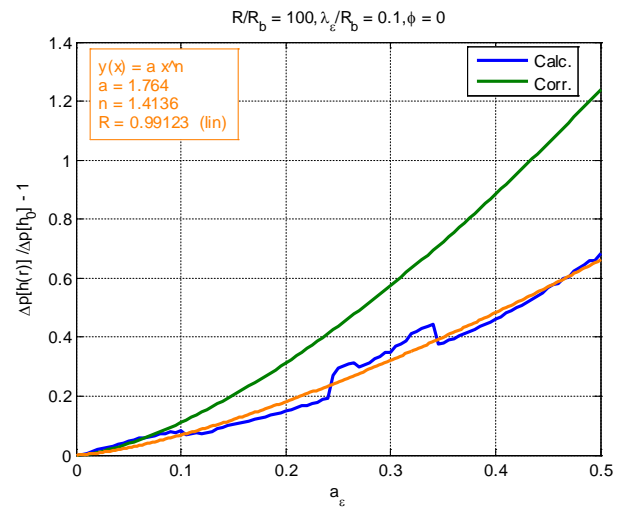


Figure 5: Relative pressure drop using the integral in Eq. (1.21) (Calc.) compared with the correlation in Eq. (1.10) (Corr.) for radial and linear (1D) geometry.

Later we may use this approach to study how e.g. the difference between converging and diverging apertures as function of radial distance.

In principle it is possible to model aperture variations also by introducing a porous zone. In ANSYS Fluent the extra pressure drop in a porous zone of length ΔL is given by:

$$\Delta p = -C_1 U \Delta L - C_2 \frac{1}{2} |U| U \Delta L \quad (0.22)$$

For Eq. (1.18) this corresponds to:

$$C_1 = f_\varepsilon \frac{12\mu}{h^2}, \quad C_2 = -\frac{6\rho}{5r} \quad (0.23)$$

Since the viscous term is the dominant one except possibly very close to the borehole we can probably safely set $C_2 = 0$. If we want to model a joint with aperture h using a geometrical model with $h = h_{geo}$ we need to subtract a contribution from this to avoid 'double-counting' since no extra friction term should be added if $h = h_{geo}$, i.e.:

$$C_1 = \frac{12\mu}{h^2} \left(f_\varepsilon - \frac{h^2}{h_{geo}^2} \right) \quad (0.24)$$

For non-Newtonian fluids this is probably difficult since then the viscosity will be velocity dependent².

4.3 Pipe flow

The flow in the borehole corresponds to pipe flow. For the given range of pumping volumes up to 30 litre/min the Reynolds number for the cement-water mixture is:

$$\text{Re}_b = \frac{\rho_{c,mix} U_{in} D_b}{\mu_{c,mix}} \leq \frac{1600 \cdot 0.22 \cdot 0.054}{0.05} \approx 380 \quad (0.25)$$

so we can assume the flow to be laminar³.

For laminar flow the pressure drop is given by:

$$\frac{\Delta p}{L} = \frac{32 \mu U_{in}}{D_b^2} = \frac{8 \mu Q}{\pi D_b^4} \quad (0.26)$$

and the entrance length to get developed flow is approximated by:

$$\frac{L_{\text{entrance}}}{D_b} \approx 0.05 \text{Re}_D, \quad \text{Re}_D = \frac{\rho U_{in} D_b}{\mu} \quad (0.27)$$

4.4 Pressure drop in bends

Neglecting friction effects the extra pressure drop into a joint due to change in the velocity direction can be estimated as:

$$\Delta p_{\text{bend}} = \frac{1}{2} \rho U^2 \frac{\Delta \theta}{90^\circ} \quad (0.28)$$

The extra pressure drop for entering a joint oriented with an angle $\theta^- = 180^\circ - \theta$ compared to an angle $\theta^+ = \theta (< 90^\circ)$ relative to the drilled hole as illustrated in Figure 6 is then:

$$\Delta p(\theta) \approx \frac{1}{2} \rho U^2 \frac{180^\circ - 2\theta}{90^\circ} = \rho U^2 \left(1 - \frac{\theta}{90^\circ} \right) \quad (0.29)$$

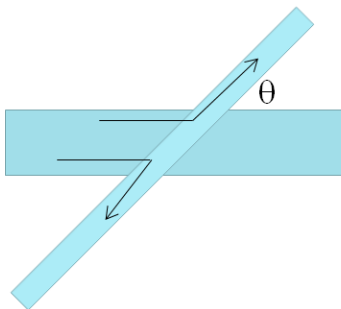


Figure 6: Joint angle relative to borehole.

² For power-law fluids possibly the variant $S_i = C_0 |U|^{c_1-1} U$ may be used.

³ For the water phase we may be slightly into the turbulent region, but the dominant factor in our case is the cement anyway since it has much higher viscosity.

The maximum occurs for $\theta \rightarrow 0$ and corresponds roughly to a borehole length:

$$L_b = \frac{\Delta p}{\frac{32\mu_{c,mix}U_{in}}{D_b^2}} = \frac{\rho_{c,mix}D_b^2U_{in}}{32\mu_{c,mix}} \sim \frac{1600 \cdot 0.05^2 \cdot 0.2}{32 \cdot 0.05} \text{ m} \sim 0.5 \text{ m} \quad (0.30)$$

or a joint length given by:

$$\frac{12\mu_{c,mix}Q}{2\pi h^3} \ln\left(1 + \frac{L_{joint}}{R_b}\right) = \Delta p \quad (0.31)$$

For $L_{joint} \ll R_b$ this simplifies to:

$$\frac{L_{joint}}{R_b} \approx \frac{\Delta p}{\frac{12\mu_{c,mix}Q}{2\pi h^3}} = \frac{\pi\rho_{c,mix}U_{in}^2}{6\mu_{c,mix}Q} h^3 \sim \frac{\pi 1600 \cdot 0.2^2}{6 \cdot 0.05 \cdot 30 \cdot \frac{1}{60 \cdot 1000}} m^{-3} h^3 \sim \left(\frac{h}{9.0 \text{ mm}}\right)^3 \quad (0.32)$$

For $h = 1 \text{ mm}$ this gives $L_{joint} \approx 0.04 \text{ mm}$. The simple order of magnitude estimate indicates that inflow of cement will be almost equal in the forward- and backward direction. Simulations will help verifying this.

4.5 Non-Newtonian fluids

For non-Newtonian fluids the viscosity is replaced by a more general rheology where the viscosity becomes a strain-rate dependent. For cement we have both a yield stress and a shear thinning behaviour. A commonly used rheology model for this type of fluid is the so called Herschel–Bulkley model or "Yield stress Power law" as shown in Figure 7

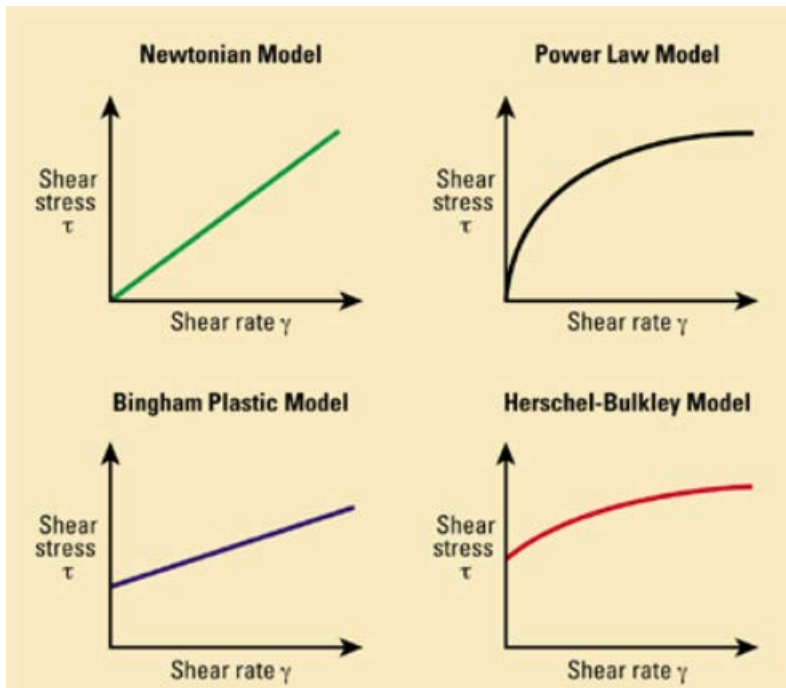


Figure 7: Typical rheology curves.

4.5.1 Herschel-Bulkley fluid

The Herschel–Bulkley rheology is defined by:

$$\tau(\dot{\gamma}) = \begin{cases} \mu_0 \dot{\gamma}, & \dot{\gamma} \leq \dot{\gamma}_0 \\ \tau_0 + K \dot{\gamma}^n, & \dot{\gamma} > \dot{\gamma}_0 \end{cases} \quad (0.33)$$

where $\dot{\gamma}_0$ is a cut-off introduced to avoid numerical problems due to infinite viscosities for vanishing strain-rates and $\mu_0 = K \dot{\gamma}_0^{n-1} + \tau_0 \dot{\gamma}_0^{-1}$ to have consistency for $\dot{\gamma} = \dot{\gamma}_0$.

4.5.1.1 Pipe flow of Herschel-Bulkley fluid

The cross-sectionally averaged velocity in a pipe with diameter D is given by, see e.g. [4]:

$$\bar{U}(\tau_{wall}) = \frac{D}{8} \left(\frac{\tau_{wall}}{K} \right)^{1/n} \frac{4n}{3n+1} (1-X)^{\frac{1}{n}} (1-aX - bX^2 - cX^3) \quad (0.34)$$

where:

$$a = \frac{1}{2n+1}, \quad b = \frac{2n}{n+1}a, \quad c = nb, \quad X = \frac{\tau_0}{\tau_{wall}} \quad (0.35)$$

Eq. (1.34) can be reformulated as:

$$\tau_{wall} = K \left(\frac{8\bar{U}}{D} \right)^n \left(\frac{3n+1}{4n} \right)^n \left(\frac{1}{1-X} \right) \left(\frac{1}{1-aX - bX^2 - cX^3} \right)^n \quad (0.36)$$

Note that:

$$\frac{dp}{dz} = -\frac{4\tau_{wall}}{D} \quad (0.37)$$

4.5.1.2 Channel flow of Herschel-Bulkley fluid

By using the same methods used to derive the pipe formulas in the previous section it can be shown that for flow between two plates with spacing h the average velocity is:

$$\bar{U}(\tau_{wall}) = \frac{h}{6} \left(\frac{\tau_{wall}}{K} \right)^{1/n} \frac{3n}{2n+1} (1-X)^{\frac{1}{n}} (1-bX - bnX^2) \quad (0.38)$$

where:

$$b = 1/(n+1), \quad X = \tau_0/\tau_{wall} \quad (0.39)$$

Eq. (1.38) can be reformulated as:

$$\tau_{wall} = K \left(\frac{6\bar{U}}{h} \right)^n \left(\frac{2n+1}{3n} \right)^n \left(\frac{1}{1-X} \right) \left(\frac{1}{1-bX - bnX^2} \right)^n \quad (0.40)$$

For radial flow with given inflow velocity U_{joint}^{in} we get:

$$\tau_{wall}(r) = K \left(\frac{6U_{joint}^{in} R_b}{h r} \right)^n \left(\frac{2n+1}{3n} \right)^n \left(\frac{1}{1-X(r)} \right) \left(\frac{1}{1-bX(r) - bnX(r)^2} \right)^n \quad (0.41)$$

where:

$$X(r) = \frac{\tau_0}{\tau_{wall}(r)} \quad (0.42)$$

We may then solve for $\tau_{wall}(r)$ numerically and get the pressure gradient as:

$$\frac{\partial p}{\partial r}(r) = -\frac{2\tau_{wall}(r)}{h} \quad (0.43)$$

The radial pressure profile is then:

$$p(r) = p_{out} + \int_r^{R_{out}} dr \frac{2\tau_{wall}(r)}{h} \quad (0.44)$$

where $p_{out} = p(r = R_{out})$ and some example profiles are shown in Figure 8. It is also possible to solve for the velocity that gives a given pressure drop from inlet to outlet:

$$\Delta p(U) = p_{in}(U) - p_{out} \quad (0.45)$$

and some examples are given in Figure 9. For a given pressure drop we can then estimate the cement front position (assuming a sharp front / plug flow) as shown in Figure 11.

Example: What is the penetration length into a joint for cements without yield stress, with 10 and 50 Pa yield stress after 10 minutes for a joint aperture of 200 μm ?

Answer: Using Figure 11 and going up from 600 seconds (roughly parallel to the left edge of the legend box) we get 10 m for the fluid without yield stress, 6 m for the fluid with 10 Pa yield stress, and for the 50 Pa yield stress case, one needs a gap above 200 μm to actuate the flow.

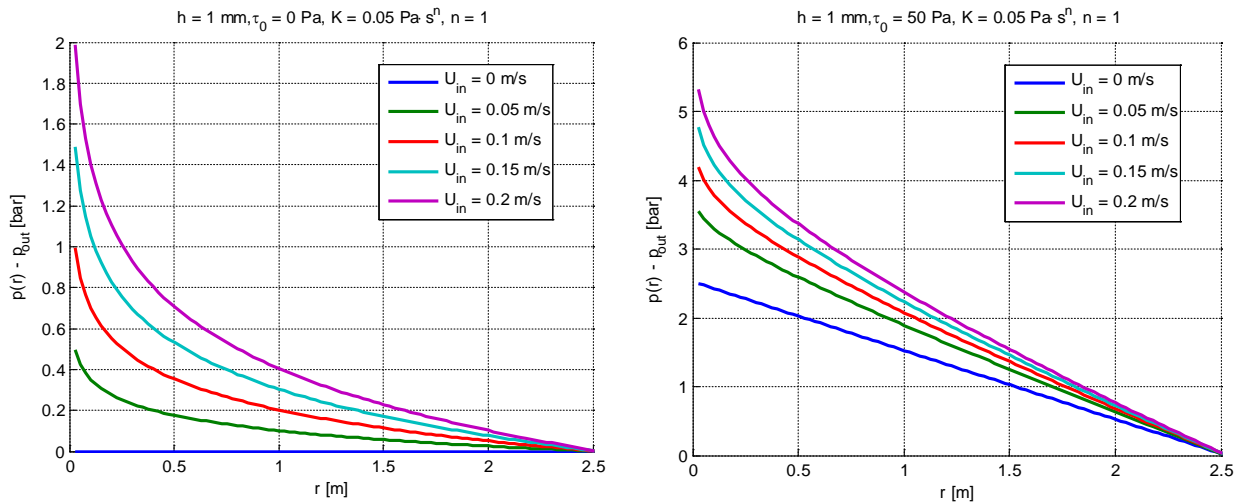


Figure 8: Radial pressure variation for Newtonian (left) and Bingham fluid (right).

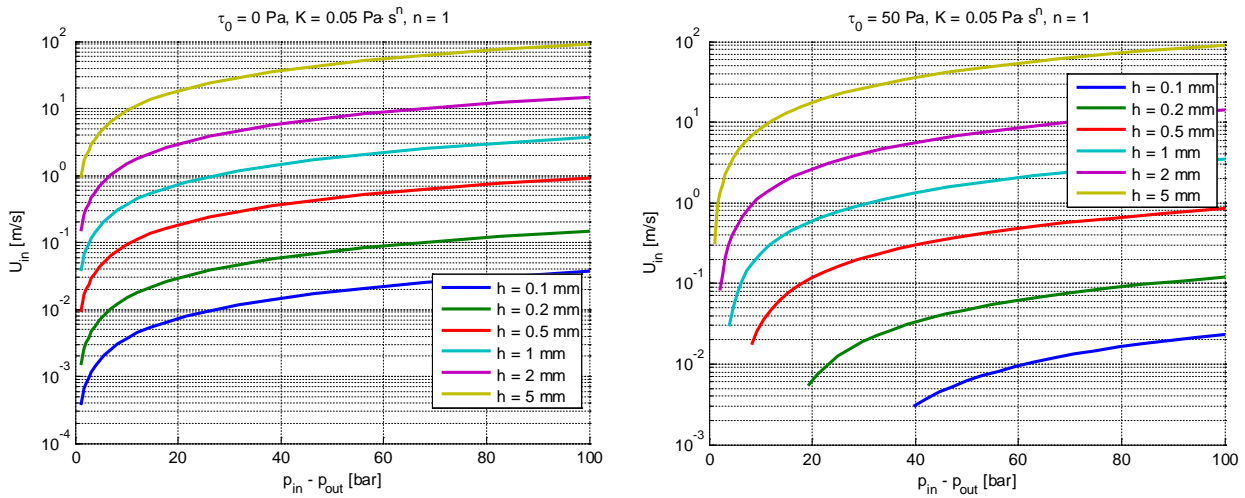


Figure 9: Inlet velocity as function of pressure drop for Newtonian (left) and Bingham fluid (right).

It is also possible to estimate the critical pressure needed to initiate flow by simply calculating the pressure needed to get a very small velocity e.g. $U = 10^{-6}$ m/s, see Figure 10. Following up on the above example, we can see that a fluid with a yield stress of 10 Pa would require a driving pressure of at least 2.5 bar in a 200 μm joint, and 25 bar for water-cement mix with a yield stress of 100 Pa. We see that for a 50 Pa yield stress mixture we would need a joint aperture of at least ~ 230 μm to actuate the flow at a pressure drop of 10 bar.

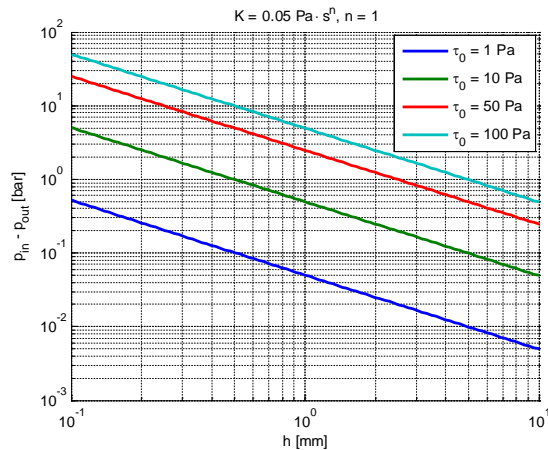


Figure 10: Critical pressure to initiate flow as function of joint aperture for different values of the yield stress for a Bingham fluid with $\mu_{pl} = K = 0.05$ Pa.s.

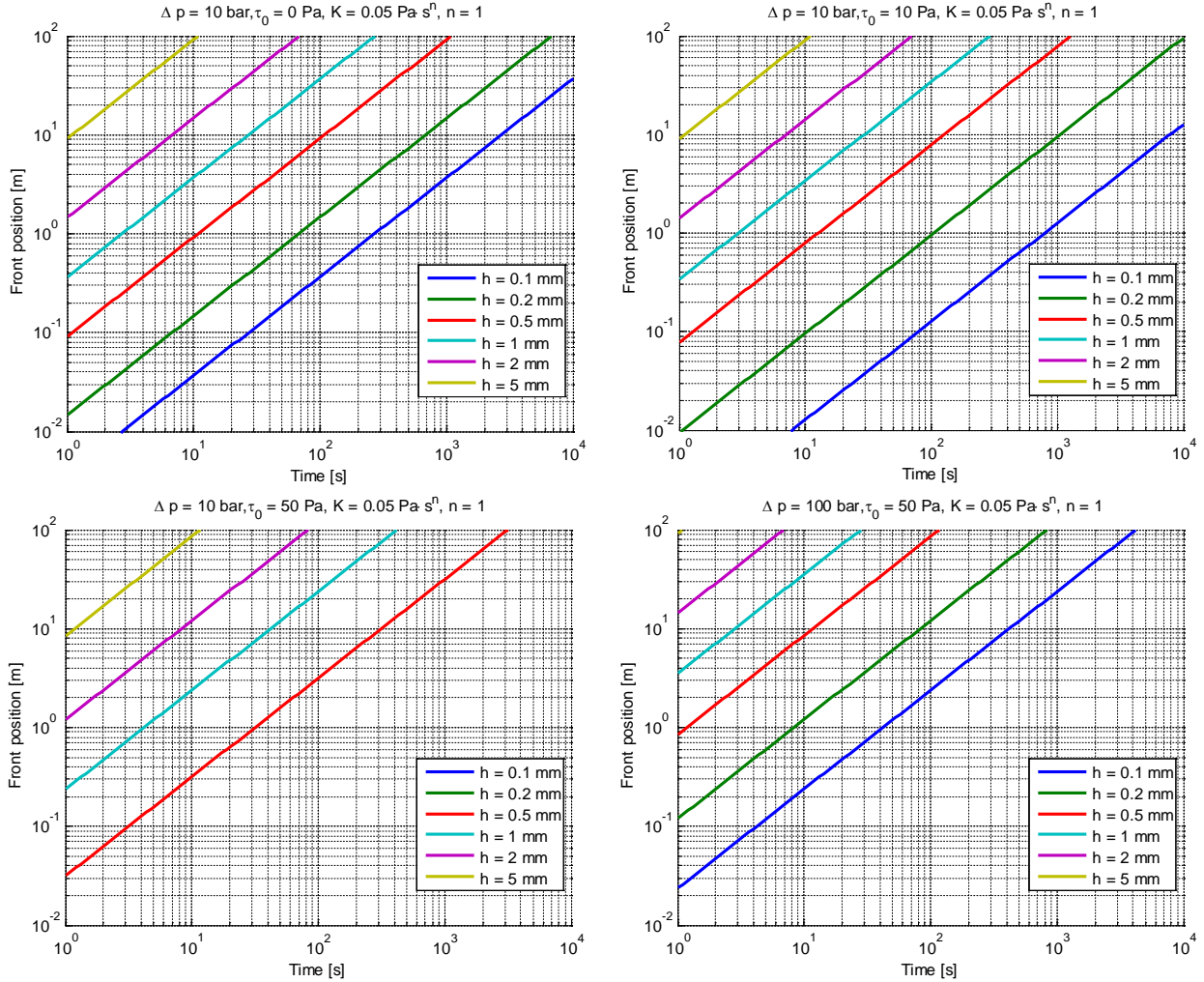


Figure 11: Front position (approximate) as function of time for different yield stresses and pressure drops for different joint apertures.

4.6 Joint spacing etc.

For a given inlet rate the joint area covered per time for a fixed aperture h is given by:

$$\frac{dA_{\text{joint}}}{dt} = \frac{Q}{h} \quad (0.46)$$

The joint area covered at a time t is:

$$A_{\text{joint}}(t) = \frac{dA_{\text{joint}}}{dt} t = \frac{Qt}{h} \quad (0.47)$$

Now assume that there are several joints along the borehole, and that all have the same fixed aperture h . For a given number of joints $N_{\text{joint}}^{\text{tot}}$ this corresponds to a radial distance:

$$R_{\text{joint}}(t) \approx \sqrt{\frac{1}{\pi N_{\text{joint}}^{\text{tot}}} \frac{dA_{\text{joint}}}{dt} t} = \sqrt{\frac{1}{\pi N_{\text{joint}}^{\text{tot}}} \frac{Qt}{h}} \quad (0.48)$$

If we assume that each joint has a radial extension R_{joint} the total number of joints crossing the borehole can be roughly estimated as:

$$N_{\text{joint}}^{\text{tot}} \sim \frac{A_{\text{joint}}}{\pi R_{\text{joint}}^2} \quad (0.49)$$

giving an estimated joint spacing of:

$$\Delta_{\text{joint}} = \frac{L_{\text{hole}}}{N_{\text{joint}}^{\text{tot}}} \quad (0.50)$$

Some examples of the above estimates are shown in Figure 12.

Example: You know the pumping rate and how long you have been pumping, this gives A_{joint} as a function of joint aperture h (Figure 12-a). Figure 12-b gives A_{joint} as a function of time for different joint apertures h . If you now know an estimate of the total number of joints along the borehole, you can estimate the penetration distance into the rock as a function of time ((Figure 12-d). If you know the penetration you can use Eq. 1.49 to estimate the number of joints, or equivalently the average separation between joints Figure 12-c as a function of joint aperture h .

Later this kind of curves may be implemented in e.g. Excel as a simple tool for the users to provide quick estimates for important joint parameters.

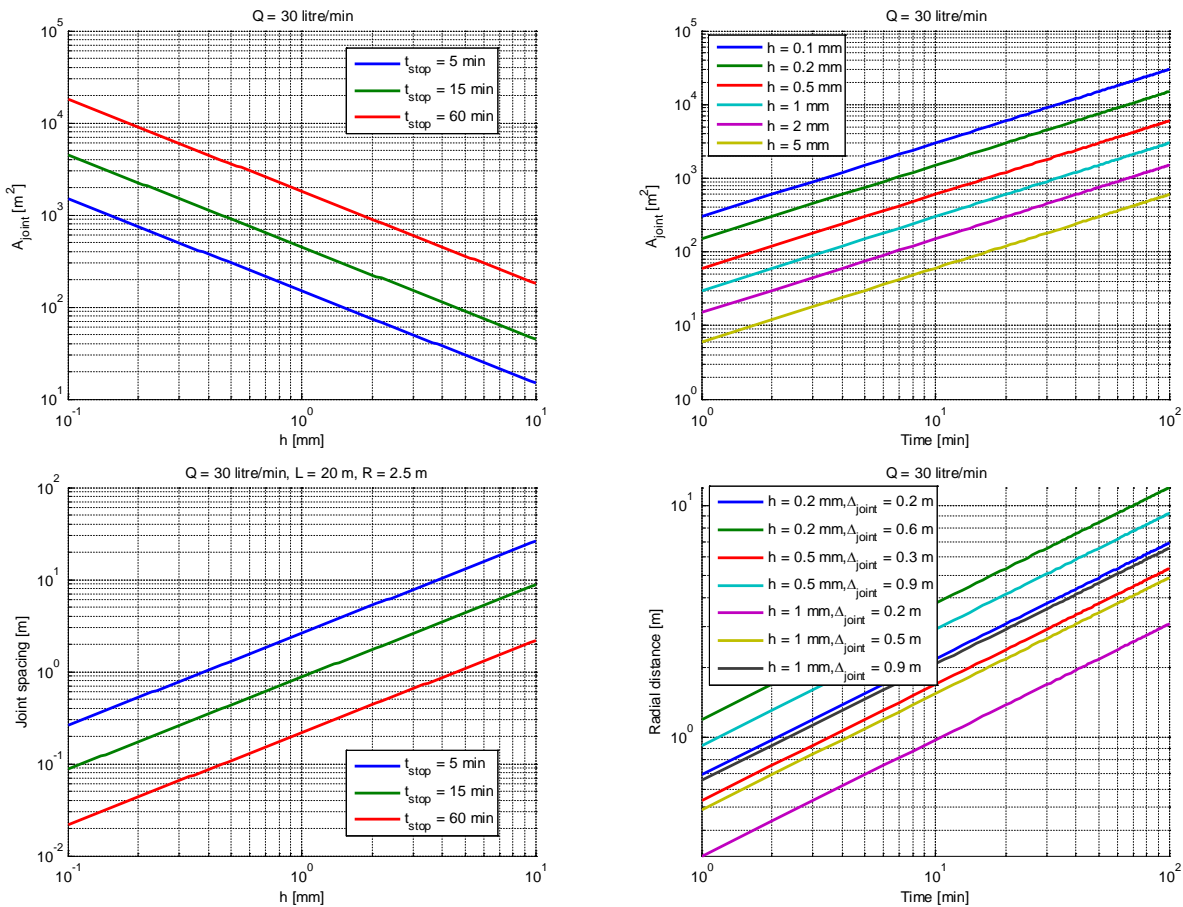


Figure 12: Joint estimates from Eq. (1.47) to Eq. (1.50).

5 ANSYS FLUENT SIMULATIONS

For the CFD simulations, using ANSYS FLUENT, the main challenge is the very large aspect ratio between the joint aperture and its radial extent. Typically, the aperture is $h < 1$ mm and the needed radius may be several meters. To resolve velocity profiles in the joint we need at least 10 cells across the joint giving a mesh size of $\Delta = h/10$. This means that we have to stretch the mesh by a large factor in the radial direction when going outwards to avoid excessive number of computational volumes. An example of the mesh refinement needed near a joint inlet is shown in Figure 13.

An important question is therefore if the geometry can be simplified without losing important physics. We therefore start by studying which phenomena dominate (and which can be neglected) and to what extent symmetry can be applied. This analysis is guided by the preceding analytical analysis. We start by single-phase flow to see what can be learned there before we extend the complexity to two-phase flow (cement replacing water).

5.1 Single phase tests

The strategy used here was to start with a full 3D model of borehole and joint to study the importance of viscous versus inertial terms. It is especially important to assess the importance of the joint angle relative to the borehole. Next, we simplified the problem by assuming that the inlet pressure to the joint can be prescribed as a boundary condition, but still retain the effect of the joint angle by using the actual cross section of the joint borehole intersection as inlet area. Thus, the problem simplifies to only the joint geometry. The effect of the joint angle then is to make the inlet more or less ellipsoidal. Next, even simpler models such as 2D and 2D-axis-symmetric models of the borehole and joint were investigated. Finally we limited the model to only the joint as a 3D disk and possible an axis-symmetric model of the disk.

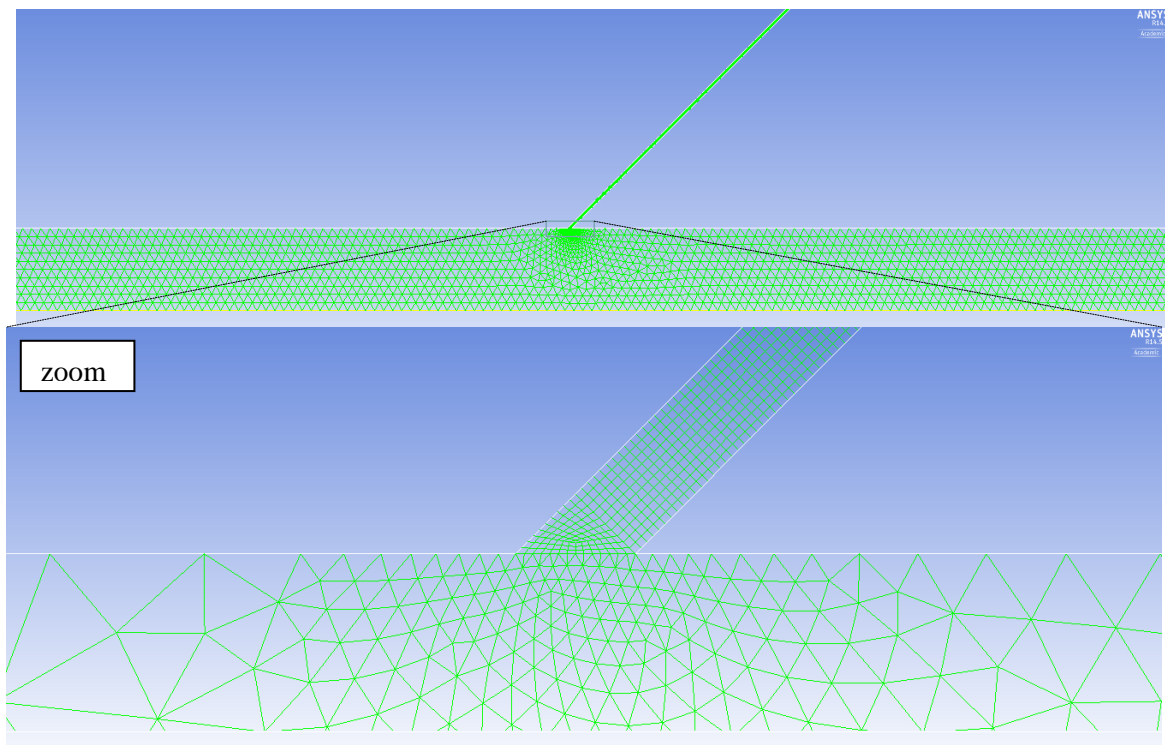


Figure 13: Mesh example

The simulations performed are summarized in **Table 5.1** and described in detail in the subsequent sections.

Table 5.1: Single phase tests

Model	Geometry	Effects
3D	Borehole+Joint	Joint angle
	Joint	Joint angle (ellipsoidal inlet)
	Joint	Joint aperture variations (porous zone)
	Joint	Joint aperture variations (modified geometry)
2D	Borehole+Joint	Joint angle
Axial	Borehole+Joint	Joint angle + Joint aperture
	Joint	Joint aperture variations (porous zone)

5.1.1 Fully 3D simulations

First we use a 3D geometry as shown in Figure 14. We study a single joint cutting a short borehole section which is closed at the distal end. An important parameter is the joint angle θ relative to the borehole.

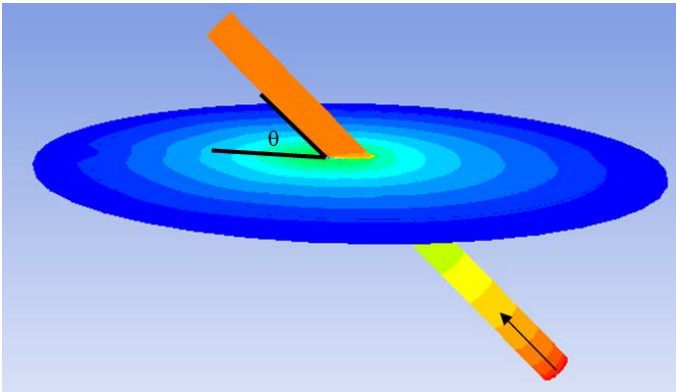


Figure 14: Single joint geometry (3D).

5.1.1.1 Effect of joint angle in simulation with both borehole and joint resolved

For high velocities and large joint apertures clearly the angle between the joint and the drilled hole will play an important role regarding inflow. However, for smaller velocities and apertures together with higher viscosities the entrance effect is expected to be reduced compared to viscous effects in the joint.

To study this we simply varied the Reynolds number:

$$\text{Re} = \frac{\rho U D}{\mu} \quad (0.51)$$

by varying the viscosity for a given case. We have used an artificially large aperture ($h \sim 10$ mm) to make an upper estimate of inertial effects compared to viscous ones. The results are shown in Figure 15. We see that by going down to $\text{Re} \sim 100$ the flow is almost axially symmetric even rather close to the ellipsoidal joint inlet.

For our case we typically have $Re < 200$ for the cement in the borehole. In addition the apertures are expected to be smaller ($h \sim 1$ mm) reducing effect of θ even more.

5.1.1.2 Effect of joint angle when simplifying to joint only being resolved

Now we study the effect of the increased joint exposure for inflow for reduced angles θ . For $|\theta| < 90^\circ$ the inflow area will get the shape of an ellipsoid. Figure 16 shows the pressure field for different angles and Figure 17 is a zoom in for the velocity field near the joint inlet. The flow pattern is clearly distorted for the smallest angles, but even then the flow becomes radial after rather short distance outwards. In Figure 18 the pressure profiles in the x- and y-directions are shown.

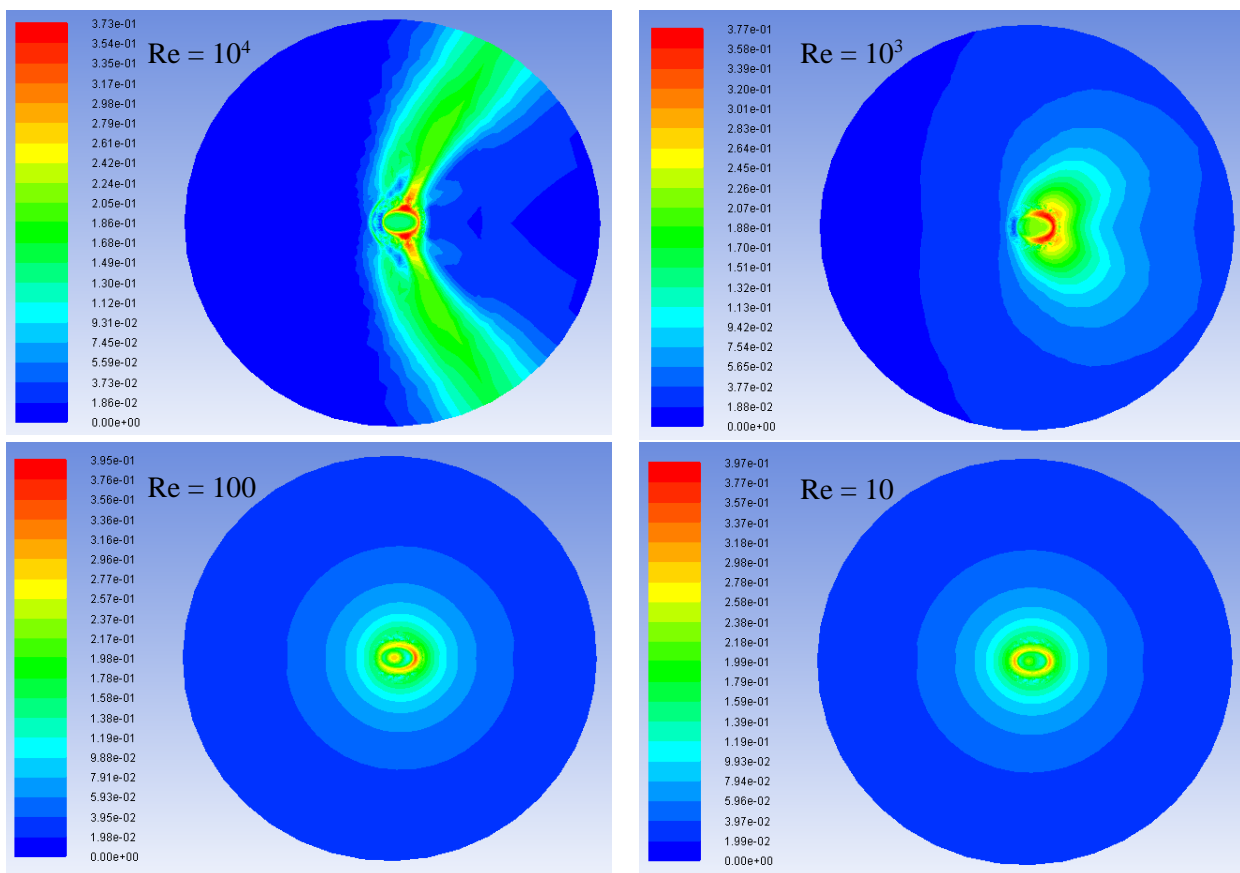


Figure 15: Velocity magnitude for single phase flow (3D, steady state, $h = 10$ mm, $\theta = 45^\circ$, $U_{in} = 0.2$ m/s) for $Re \sim [10^4, 10^3, 100, 10]$ from top left to bottom right. The diameter here is $D_{joint} = 1.0$ m.

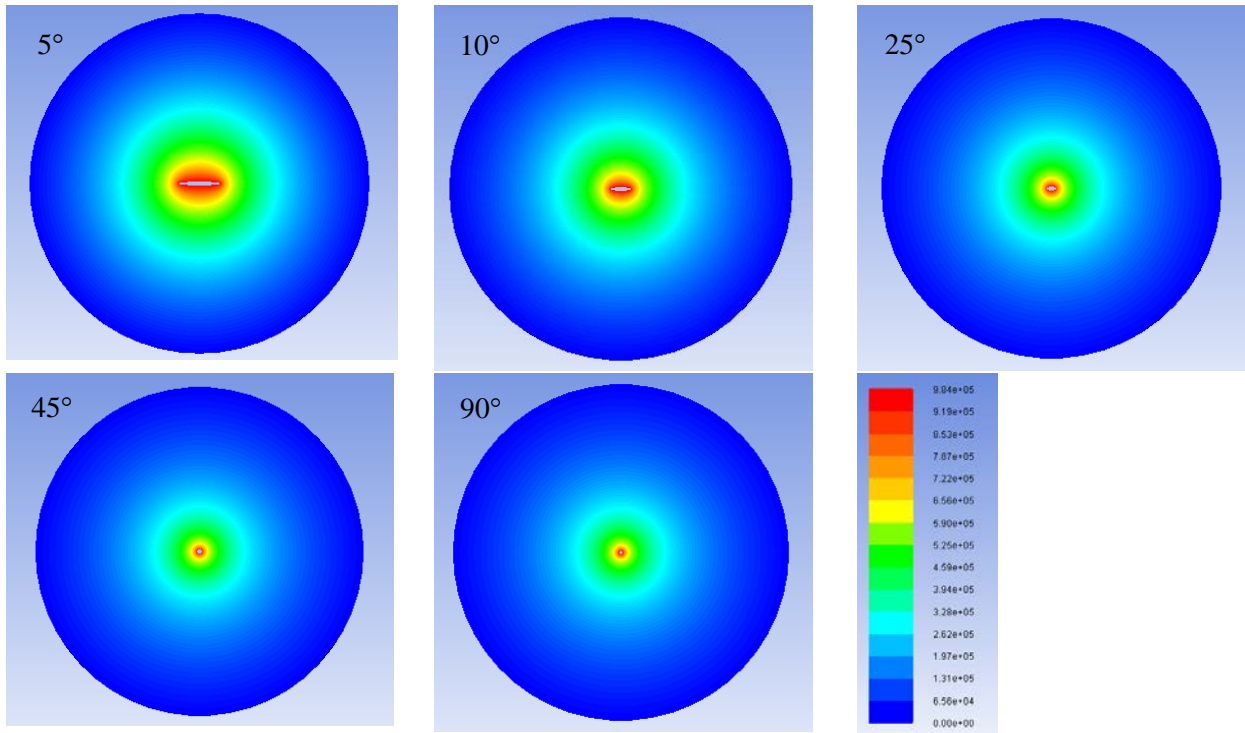


Figure 16: Pressure for single phase flow (3D-Joint only, steady state, $h = 1$ mm, $p_{in} = 10$ bar, $\rho = 1000$ kg/m³, $\mu = 0.1$ Pa·s) for $\theta = [5^\circ, 10^\circ, 25^\circ, 45^\circ, 90^\circ]$. The diameter here is $D_{joint} = 5.0$ m. The colorscale is the same for all the figures.

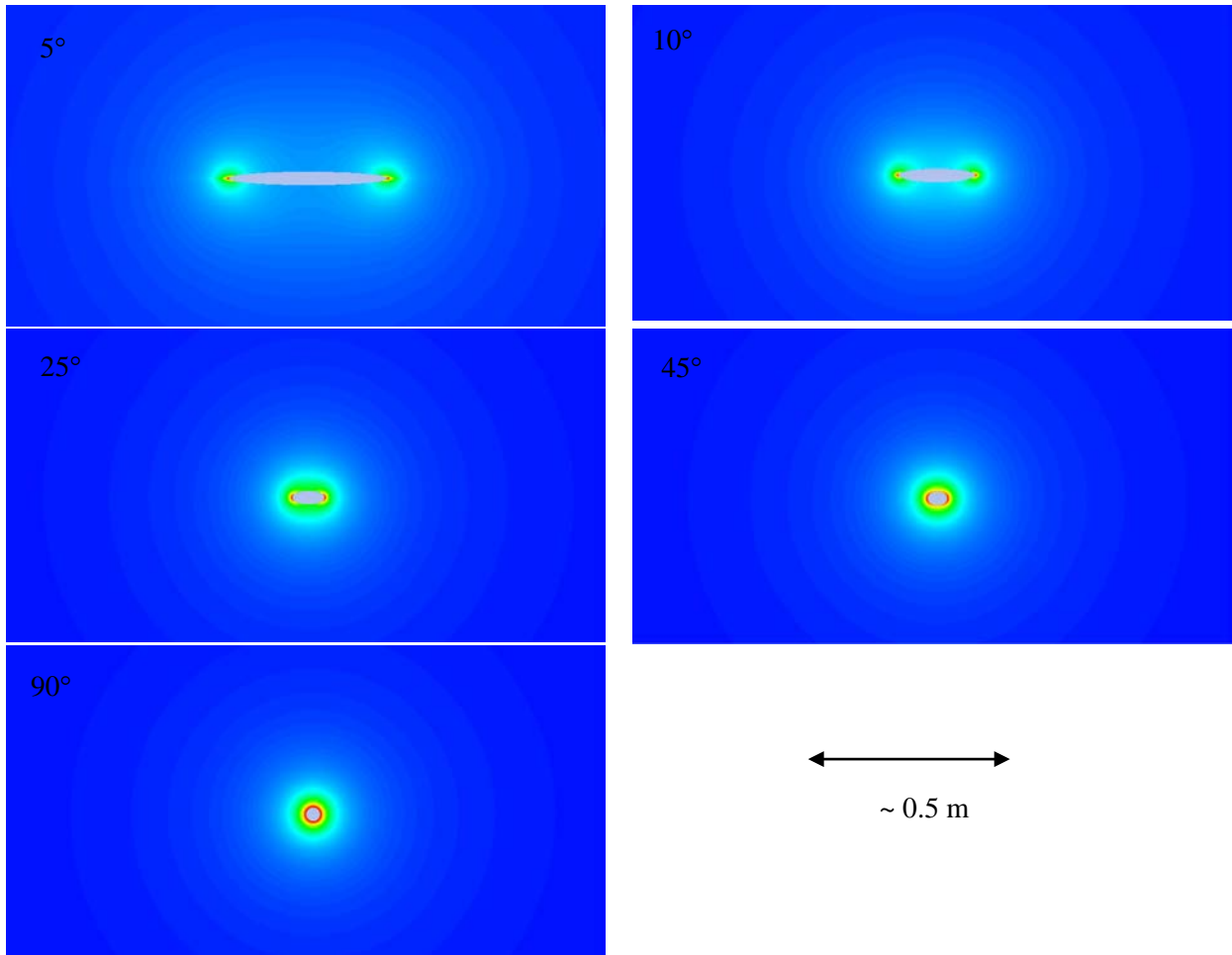


Figure 17: Velocity magnitude for single phase flow (3D-Joint only, steady state, $h = 1 \text{ mm}$, $p_{in} = 10 \text{ bar}$, $\rho = 1000 \text{ kg/m}^3$, $\mu = 0.1 \text{ Pa}\cdot\text{s}$) for $\theta = [5^\circ, 10^\circ, 25^\circ, 45^\circ, 90^\circ]$.

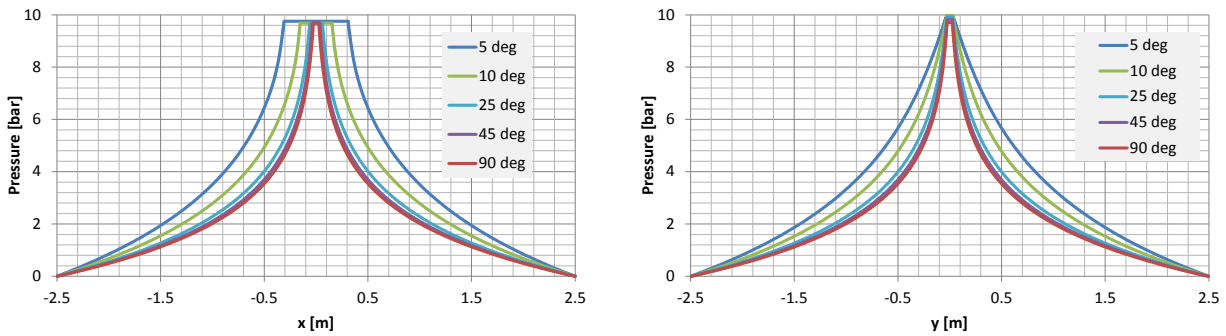


Figure 18: Pressure profiles (x- and y-axis) for cases shown in Figure 16.

In Figure 19 the volume flow rate is shown as function of angle. As expected the flow rate increases for smaller angles due to the increased exposure area of the joint to the borehole. The effect appears to be rather small ($< 10\%$) for $\theta \geq 30^\circ$. With smaller angle, the communicating area between drill hole and joint are larger, so it help to increase the grout flow. It means that in an extreme case, where the joint cutting along the drill hole we will have maximum area and thereby maximum flow.

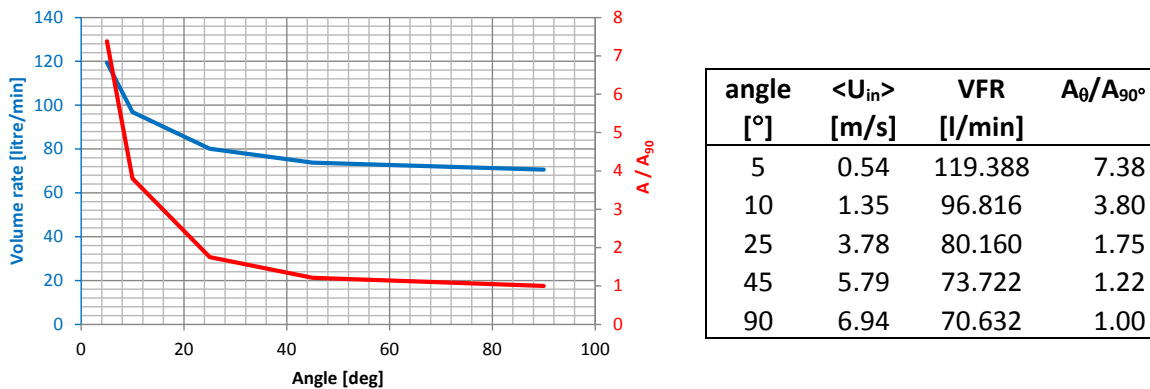


Figure 19: Volume flow rate for single phase flow (3D-Joint only, steady state, $h = 1$ mm, $p_{in} = 10$ bar, $\rho = 1000$ kg/m³, $\mu = 0.1$ Pa·s) as function of θ .

5.1.2 Reduced dimensionality – 2D

5.1.2.1 Joint angle

We also did a test in 2D (planar) to test the effect of the angle θ . We fixed the inlet pressure to $p_{in} = 10$ bar and measured the inflow. The results are shown in Figure 20 and Table 5.3. We see that the inflow is almost identical for the forward and backward pointing joint, i.e. θ and $180^\circ - \theta$. For $\theta = 175^\circ$ we observe a vortex outside the joint inlet not present for $\theta = 5^\circ$, but even this seems to have minimal effect on the inflow. The conclusion therefore is that the added pressure drop due to change of flow direction is negligible compared to the viscous pressure drop inside the joint. Also the inflow is almost the same for all angles $\theta = [5^\circ, 45^\circ, 90^\circ, 135^\circ, 175^\circ]$.

Table 5.2: Inlet velocity for single phase flow (2D, steady state, $h = 1$ mm, $p_{in} = 10$ bar, $\rho = 1000$ kg/m³, $\mu = 0.1$ Pa·s) for $\theta = [5^\circ, 45^\circ, 90^\circ, 135^\circ, 175^\circ]$.

Angle [°]	U_{in} [m/s]
5	0.01269
45	0.01268
90	0.01261
135	0.01262
175	0.01266

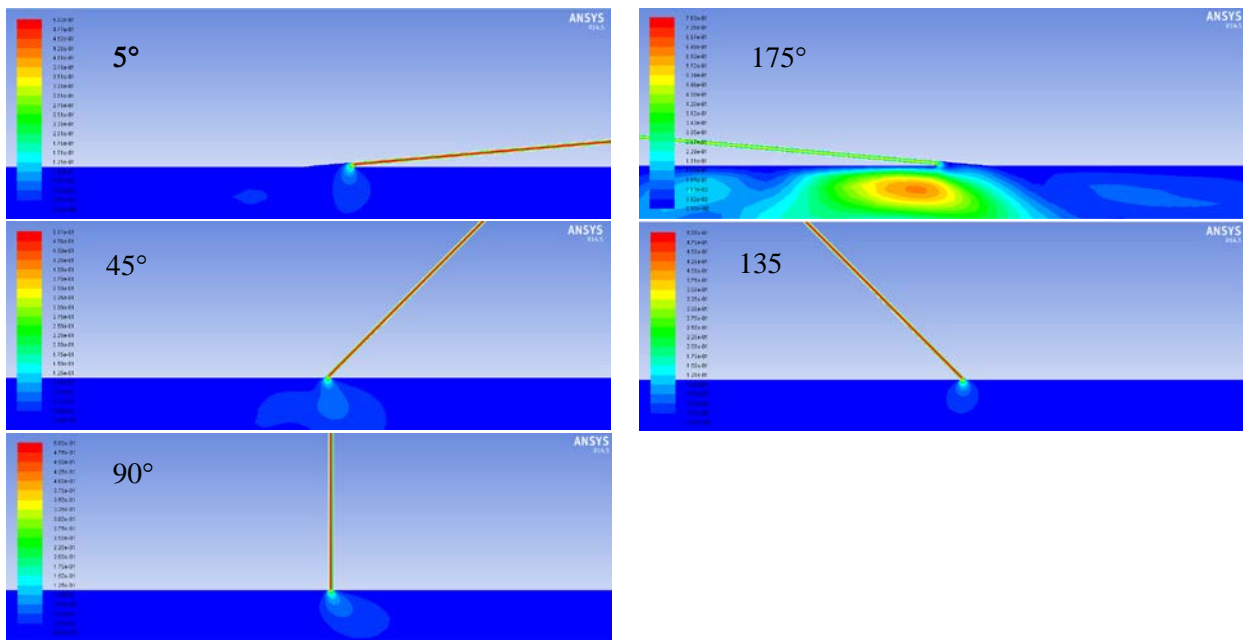


Figure 20: Velocity magnitude for single phase flow (2D, steady state, $h = 1$ mm, $p_{in} = 10$ bar, $\rho = 1000$ kg/m³, $\mu = 0.1$ Pa·s) for $\theta = [5^\circ, 45^\circ, 90^\circ, 135^\circ, 175^\circ]$.

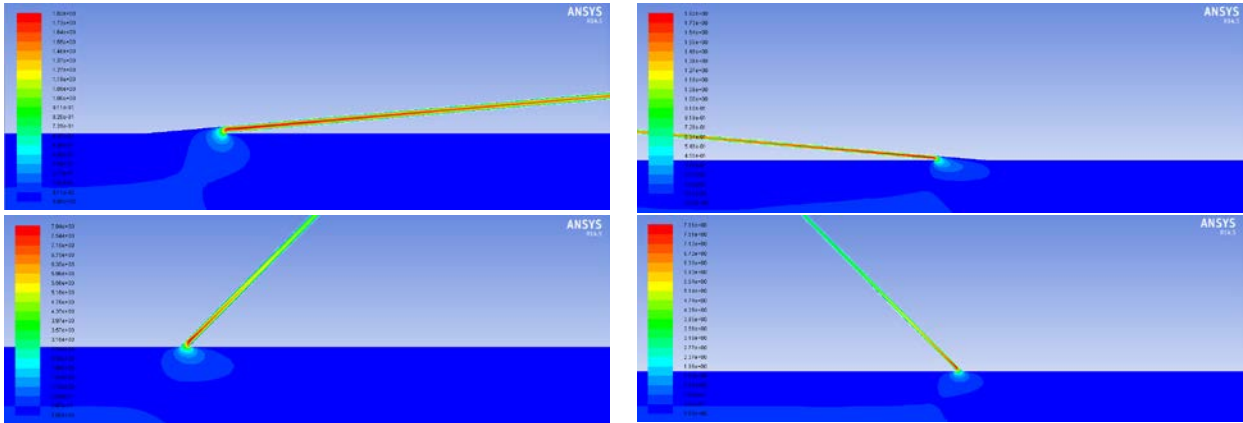


Figure 21: Velocity magnitude for single phase flow (Axis symmetric, steady state, $h = 1 \text{ mm}$, $p_{in} = 10 \text{ bar}$, $\rho = 1000 \text{ kg/m}^3$, $\mu = 0.1 \text{ Pa}\cdot\text{s}$) for $\theta = [5^\circ, 45^\circ, 135^\circ, 175^\circ]$.

5.1.3 Axis symmetric 3D model

In planar 2D we loose the effect of increasing volume/area when going outwards from the hole. Another simplified model is to use an axis symmetric model, i.e. a 2D model rotated around the centre axis of the hole.

5.1.3.1 Joint angle

First we study the potential difference between angles θ and $180^\circ - \theta$ also here. Clearly the general comparison between the different angles outside the pair $[\theta, 180^\circ - \theta]$ is meaningless here due to the distorted joint geometry. We fix the inlet pressure to $p_{in} = 10 \text{ bar}$ and measure the inflow. The results are shown in Figure 21 and Table 5.3. We see that the inflow is almost identical for the forward and backward pointing joint. The added pressure drop for change of flow direction is therefore negligible compared to the viscous pressure drop in the joint.

Table 5.3: Inlet velocity/flow rate for single phase flow (Axis symmetric, steady state, $h = 1 \text{ mm}$, $p_{in} = 10 \text{ bar}$, $\rho = 1000 \text{ kg/m}^3$, $\mu = 0.1 \text{ Pa}\cdot\text{s}$) for $\theta = [5^\circ, 45^\circ, 90^\circ, 135^\circ, 175^\circ]$.

Angle [°]	$U_{in} \text{ [m/s]}$	$Q_{in} \text{ [l/min]}$
5	0.0940	12.9
45	0.3945	54.2
90	0.5147	70.7
135	0.3948	54.3
175	0.0939	12.9

5.1.3.2 Joint aperture

The most important parameter is the joint aperture. Since the angle has been shown to play a minor effect we limit ourselves to $\theta = 90^\circ$ and vary the aperture from $h = [0.1, 0.5, 1.0, 2.0]$ mm. The results are summarized in Table 5.4 and compared with the theoretical estimate from Eq. (1.14) in Figure 22. The ANSYS Fluent results almost perfectly match the analytical model.

Table 5.4: Pressures (inlet + joint-inlet) for single phase flow (Axis symmetric, steady state, $\theta = 90^\circ$, $U_{in} = 0.2$ m/s, $\rho = 1000$ kg/m³, $\mu = 0.1$ Pa·s) for $h = [0.1, 0.5, 1.0, 2.0]$ mm.

h [mm]	p_{in} [bar]	$p_{frac-inlet}$ [bar]
0.10	3094.3	3888.7
0.25	249.419	248.507
0.50	31.214	30.984
1.00	3.912	3.852
2.00	0.492	0.476

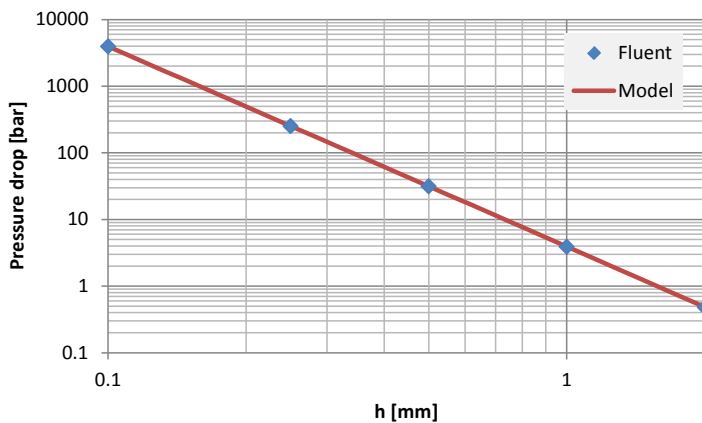


Figure 22: Pressure drop as function of aperture h – Comparison of ANSYS Fluent results (axis symmetric,) and the model given in Eq. (1.14).

5.1.3.3 Joint aperture variations – Porous zone

To include spatial aperture variations we may change the geometry of the joint. However it is also possible to emulate many of the most important effects of varying joint aperture by using a porous zone as mentioned in Section 4.2.1. The equations solved are then modified as described in Figure 23.

Note that we simply varied the porosity/permeability over the whole cross-section/aperture (z-direction) in a 3D model. Another possibility would be to block parts of the aperture by introducing cells with very low porosity/permeability at the walls.

Using the physical velocity formulation, and assuming a general scalar ϕ , the governing equation in an isotropic porous media has the following form:

$$\frac{\partial(\gamma\rho\phi)}{\partial t} + \nabla \cdot (\gamma\rho\vec{v}\phi) = \nabla \cdot (\gamma\Gamma\nabla\phi) + \gamma S_\phi \quad (6.35)$$

Assuming isotropic porosity and single phase flow, the volume-averaged mass and momentum conservation equations are as follows:

$$\frac{\partial(\gamma\rho)}{\partial t} + \nabla \cdot (\gamma\rho\vec{v}) = 0 \quad (6.36)$$

$$\frac{\partial(\gamma\rho\vec{v})}{\partial t} + \nabla \cdot (\gamma\rho\vec{v}\vec{v}) = -\gamma\nabla p + \nabla \cdot (\gamma\vec{\tau}) + \gamma\vec{B}_f - \left(\frac{\gamma^2\mu}{K}\vec{v} + \frac{\gamma^3C_2}{2}\rho|\vec{v}|\vec{v} \right) \quad (6.37)$$

Figure 23: Porous zone equations (from the Fluent Users Guide).

As a base case we use an *axially symmetric* case with $h_0 = 2$ mm and tried to emulate smaller apertures by modifying porosity and permeability. A stepwise approach was used:

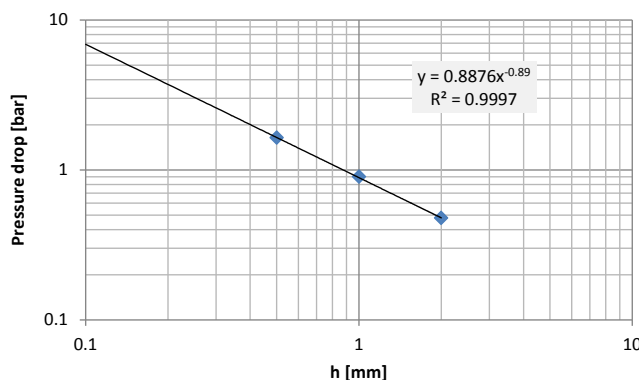
1. Only porosity, $\phi(x, y) = h(x, y)/h_0$
2. Only permeability, $k(x, y) = h^2(x, y)/12$ (*)
3. Both porosity and permeability

(*) To avoid 'double counting' we have to subtract the original contribution:

$$\frac{1}{k} = \frac{12}{h^2} \left[1 - \left(\frac{h}{h_0} \right)^2 \right] \quad (0.52)$$

1) Only porosity:

For only porosity changes we get the results in Figure 24. For the smallest apertures/porosities we experienced numerical stability issues. It therefore seems that going below a porosity of ~25% should be avoided. The pressure drop scales roughly as $\Delta p \sim h^{-1}$.

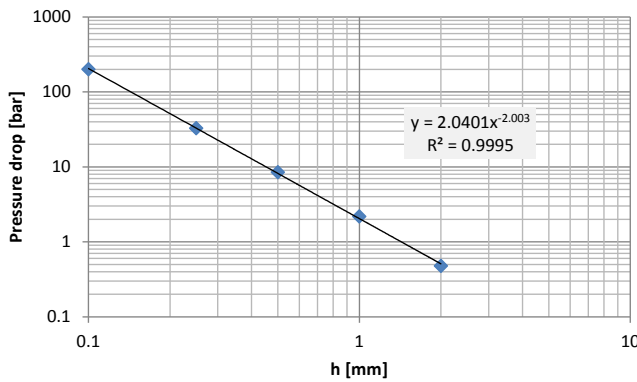


h_{Target} [mm]	Por. [-]	$1/K$ [10^6 m^{-2}]	p_{in} [bar]	$p_{\text{frac-in}}$ [bar]
0.10	0.050	0	-	-
0.25	0.125	0	-	-
0.50	0.250	0	1.800	1.634
1.00	0.500	0	0.946	0.899
2.00	1.000	0	0.492	0.476

Figure 24: Pressure drop for single phase flow (Axial-Joint only, steady state, $\theta = 90^\circ$, $U_{\text{in}} = 0.2$ m/s, $\rho = 1000$ kg/m³, $\mu = 0.1$ Pa·s, $h_0 = 2.0$ mm) for different apertures h modified via porosity changes.

2) Only permeability:

For only permeability changes we get the results in Figure 25. For the smallest apertures/porosities we again experienced some numerical stability issues, but here we were able to get some results. The pressure drop scales roughly as $\Delta p \sim h^{-2}$.



h_{Target} [mm]	Por. [-]	$1/K$ [10^6 m^{-2}]	p_{in} [bar]	$p_{\text{frac-in}}$ [bar]
0.10	1	1197	199.64	199.63
0.25	1	189	32.672	32.658
0.50	1	45	8.502	8.487
1.00	1	9	2.187	2.172
2.00	1	0	0.492	0.476

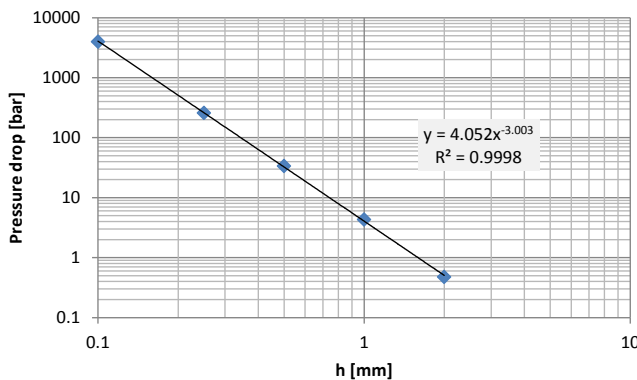
Figure 25: Pressure drop for single phase flow (Axial-Joint only, steady state, $\theta = 90^\circ$, $U_{\text{in}} = 0.2 \text{ m/s}$, $\rho = 1000 \text{ kg/m}^3$, $\mu = 0.1 \text{ Pa}\cdot\text{s}$, $h_0 = 2.0 \text{ mm}$) for different apertures h via permeability changes.

3) Both porosity and permeability:

For both porosity and permeability variations we get the results in Figure 26. For the smallest apertures/porosities we again experienced some numerical stability issues, but here we were able to get some results. The pressure drop scales roughly as $\Delta p \sim h^{-3}$. Note that here we have to use:

$$\frac{1}{K} = \frac{12}{\phi h^2} \left[1 - \left(\frac{h}{h_0} \right)^2 \right] \quad (0.53)$$

due to the presence of the $\gamma^2 \equiv \phi^2$ term in the friction part of Eq. 6.37 in Figure 23.



h_{Target} [mm]	Por. [-]	$1/K$ [10^6 m^{-2}]	p_{in} [bar]	$p_{\text{frac-in}}$ [bar]
0.10	0.050	23940	3980.93	3976.69
0.25	0.125	1512	259.772	259.096
0.50	0.250	180	33.717	33.546
1.00	0.500	18	4.338	4.292
2.00	1.000	0	0.492	0.476

Figure 26: Pressures (inlet + joint-inlet) for single phase flow (Axial-Joint only, steady state, $\theta = 90^\circ$, $U_{\text{in}} = 0.2 \text{ m/s}$, $\rho = 1000 \text{ kg/m}^3$, $\mu = 0.1 \text{ Pa}\cdot\text{s}$, $h_0 = 2.0 \text{ mm}$) for different apertures h modelled via porosity- and permeability changes.

5.1.4 Full 3D model of joint:

To pursue this further we generate a roughness landscape in Matlab and use this as input to ANSYS Fluent. An example is shown in Figure 27. Velocity contours are shown in Figure 28. We clearly see that the effect of the roughness decreases when going outwards from the borehole. This is as expected for a radial geometry. For comparison we show a result for a square geometry in Figure 29 where the whole bottom edge is inlet and the whole top edge is outlet.

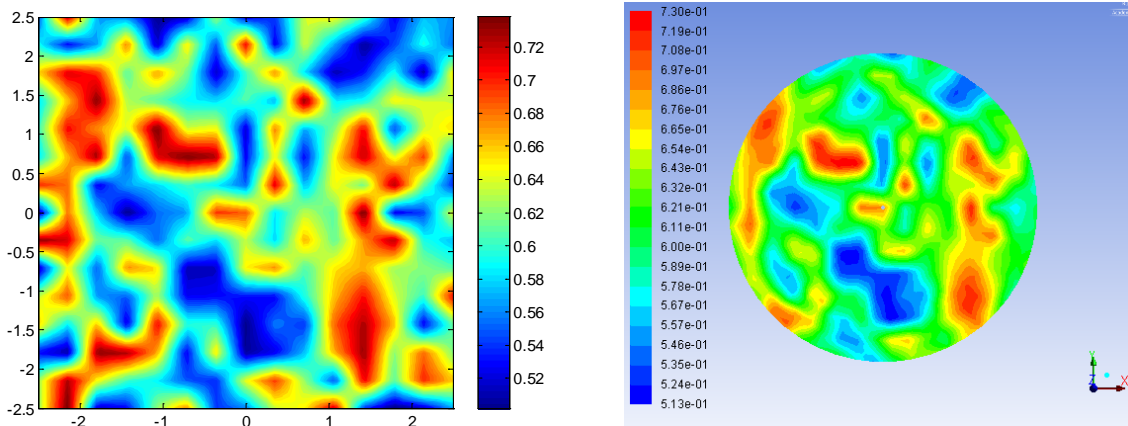


Figure 27: Relative joint aperture $h(x, y)/h_0$ from Matlab (left) and Fluent (right).

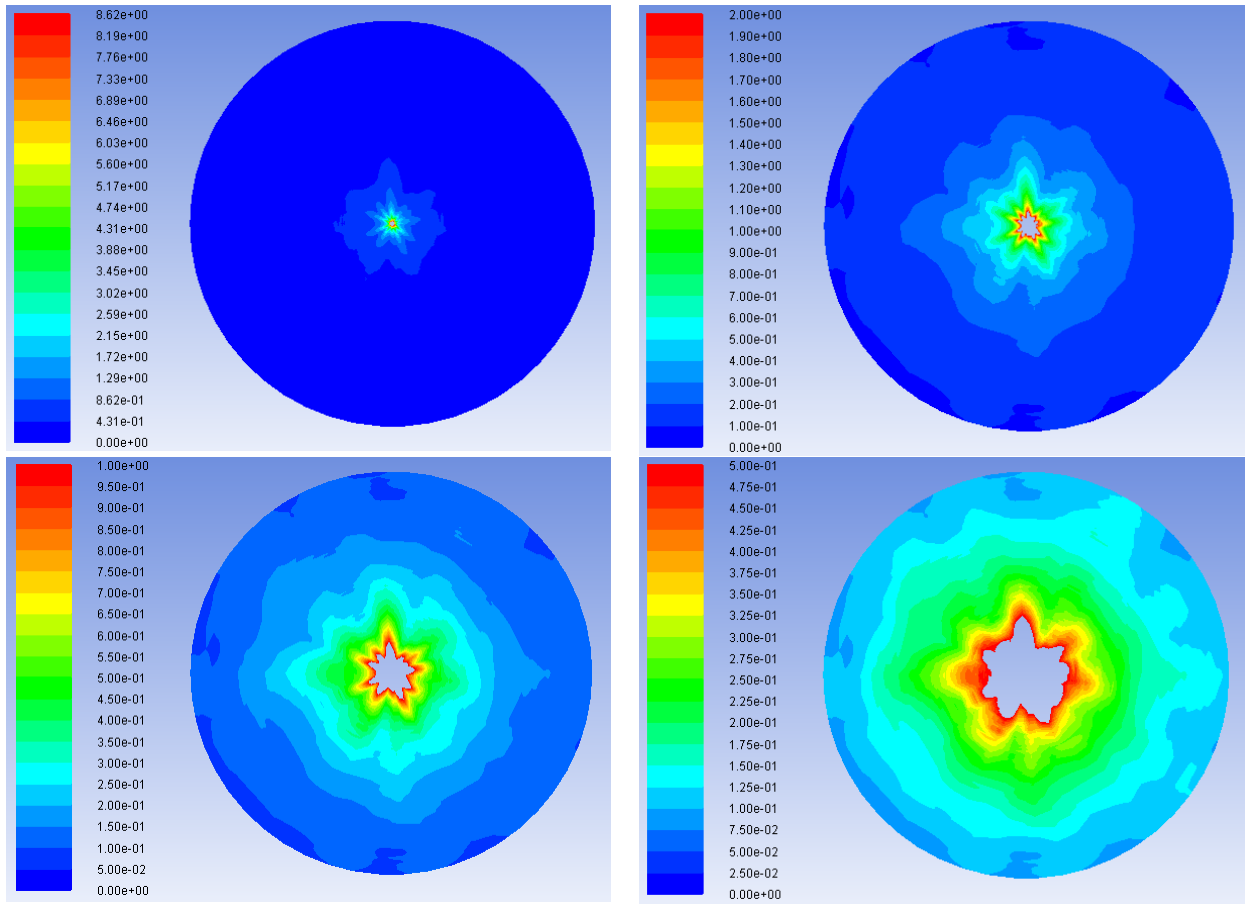


Figure 28: Velocity magnitude for different velocity ranges (3D-Joint only). Velocities exceeding the maximum value defined by the colorbar in each figure are not plotted.

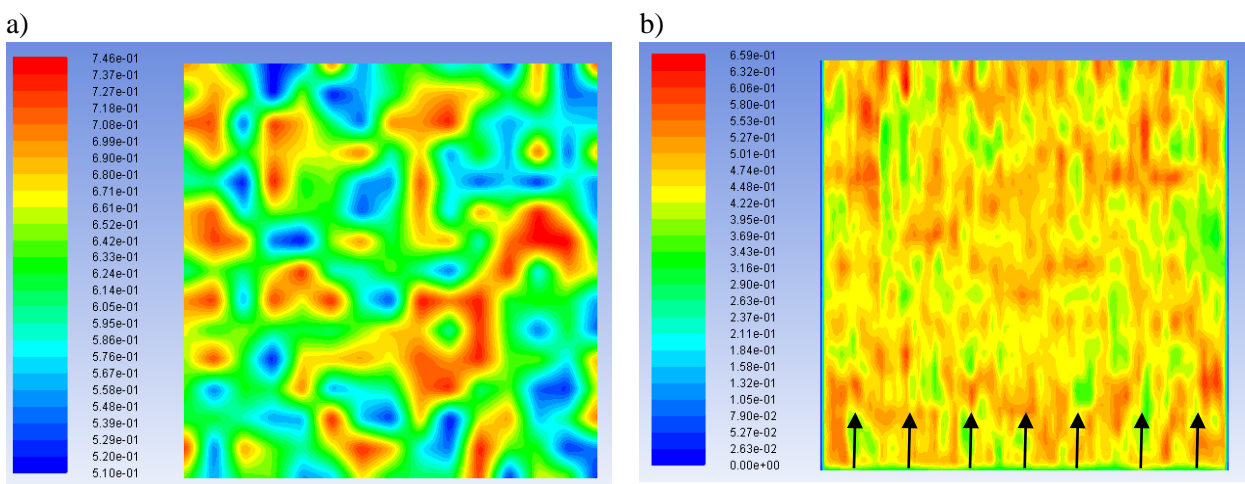


Figure 29: Flow in square joint (3D-Joint only) - a) porosity $h(x, y)/h_0$, b) velocity magnitude. The flow direction is from the lower edge to the upper edge.

5.1.4.1 Joint aperture variations – Modified geometry

Here we generate stochastic joint planes and create new mesh for each geometry realization. In Figure 30 we show results for cases generated with nominal hydraulic aperture $h = 1$ mm, with Gaussian variation in local aperture with standard deviation $\sigma_h = 0.3162$ mm. Cut outs in the upper row indicate that the region is occupied by rock.

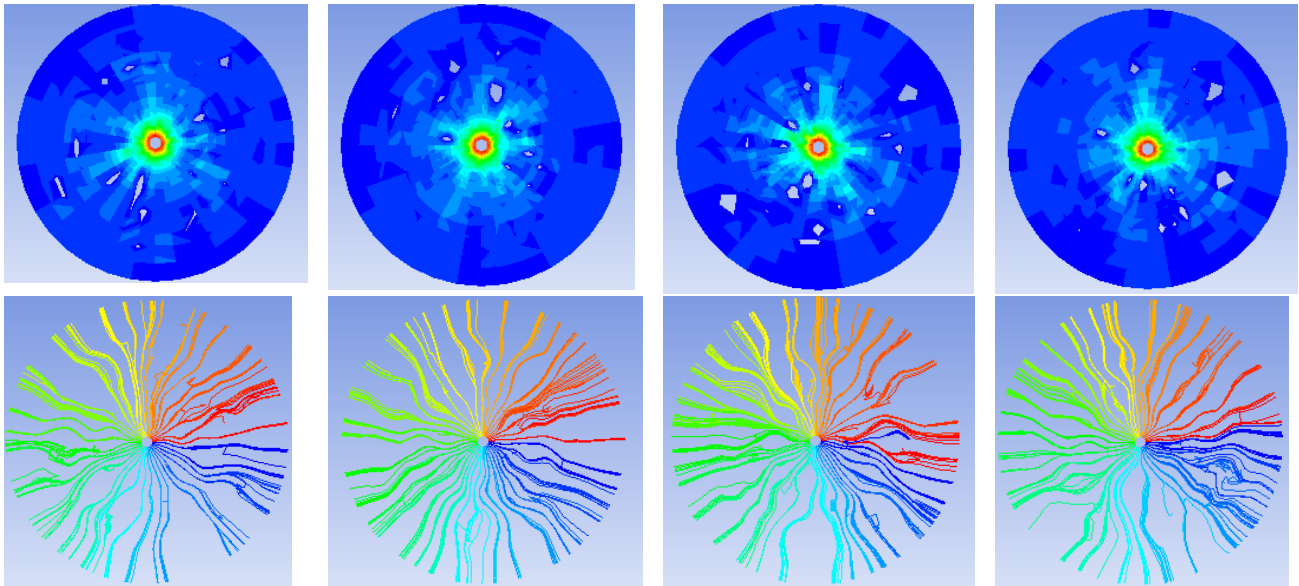


Figure 30: Contour plots of velocity [Inlet velocity 0.5 m/s (red) – nominal outlet velocity 1 mm/s (dark blue)] and path line plots (tracers injected from the inlet colored by path id). Model: 3D-Joint only.

5.1.4.2 Joint aperture variations – Ensemble averaging

Since joint aperture variations are stochastic in nature it is essential to be able to run a rather large number of cases to get statistical significant results. Both the approaches above (porous zone and stochastic joint planes) are possible to automatize as indicated in Figure 31 allowing large number of case to be run without excessive manual effort.

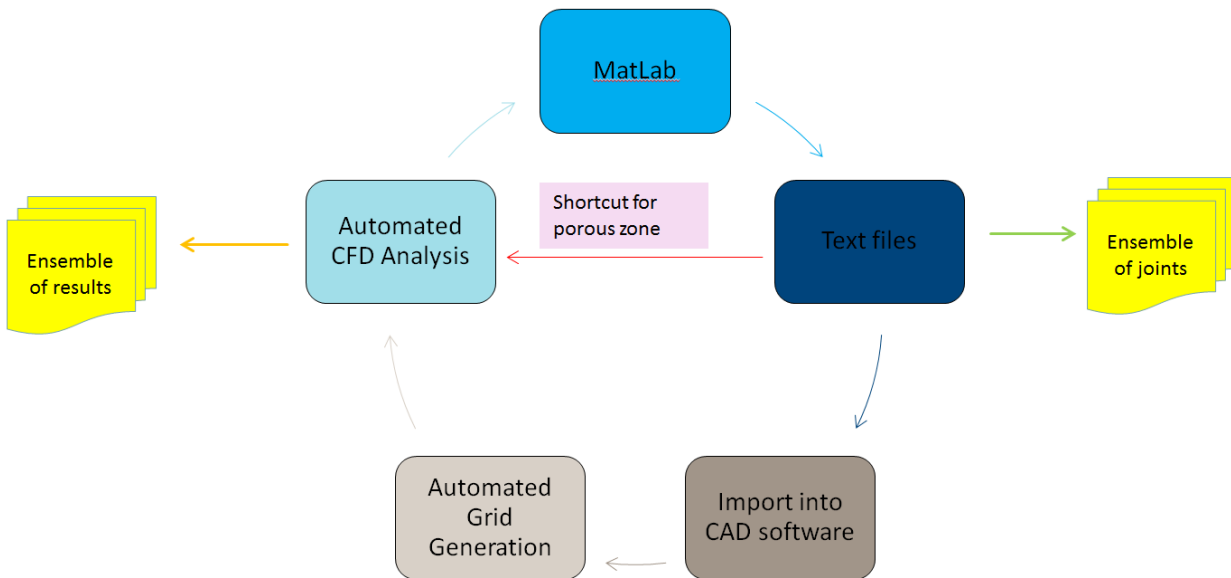


Figure 31: Workflow for analysis in stochastic joint sets – need to perform ensemble analysis.

5.1.5 Non-Newtonian single phase fluid

The first test for non-Newtonian fluid flow was to study a cases with increasing yield stress for a fixed inlet flow rate. Here we expect increased pressure drop in accordance with Eq. (1.44).

In Table 5.5 the pressures at the borehole inlet and the joint inlet are shown for different values of the yield stress for a Bingham fluid. The inlet velocity is fixed at $U_{in} = 0.2$ m/s (The joint inlet velocity is then $U_{joint}^{in} = U_{in}d/4h$). We see that the results are close to Eq. (1.44), but generally slightly lower for reasons unknown at the time of writing.

Table 5.5: Pressures (inlet + joint-inlet) for single phase flow (Axis-symmetric, steady state, $\theta = 90^\circ$, $h = 1$ mm, $U_{in} = 0.2$ m/s, $\rho = 1000$ kg/m³, $\mu = 0.1$ Pa·s) for $\tau_0 = [0.0, 10.0, 100.0]$ Pa.

τ_0 [Pa]	p_{in} [bar]	$p_{frac-inlet}$ [bar]	p_{drop} [bar] - Eq. (1.44)
0.0	3.91	3.85	3.97
10.0	4.70	4.63	4.71
100.0	10.39	10.29	10.66

5.2 Cement replacing water (2-phase, Fluent)

Now we turn to cement injection to displace the water present. This means that the hole and joint is initially filled with water and then cement is injected into the system gradually replacing the water. This is a two-phase problem and we use the Volume of fluid (VOF) model in ANSYS Fluent. It is an interface modelling technique, i.e. a numerical technique for tracking and locating the fluid-fluid interface as illustrated in Figure 32. The method is best suited to handle cases with well defined large-scale-interfaces between the phases (as in our case) in contrast to cases with one phase dispersed as small droplets in the other. If interfacial tension between the phases is neglected the water and cement will have the same pressure at a given position (but dropping from the inlet to the outer boundary, dependent on the flow).

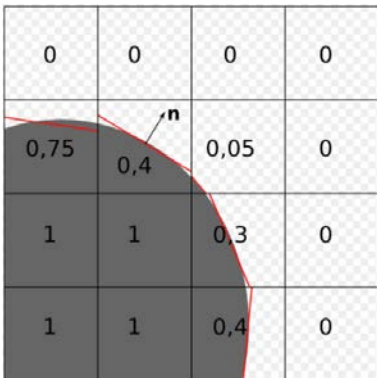


Figure 32: Schematic representation of interface reconstruction used in VOF (with PLIC -Piecewise linear construction – method). The numbers represent the "grey phase" volume fractions.

As shown for the single-phase model the dominant effect is the aperture h . In addition an effect is expected for small angles θ due to the enlarged elliptic interfacial area between the hole and the joint.

5.2.1 3D Axis symmetric – Newtonian

5.2.1.1 Joint angle

First we also here did an axis symmetric test to investigate the effect of joint angle for a case with $h = 1$ mm. From the results in Figure 33 we see that the inlet pressure when the cement has started to flow into the joint is very similar for the joints with angles θ and $180^\circ - \theta$.

NB! The joint areas are distorted due to the axis symmetry. Therefore only angle pairs θ and $180^\circ - \theta$ should be compared here.

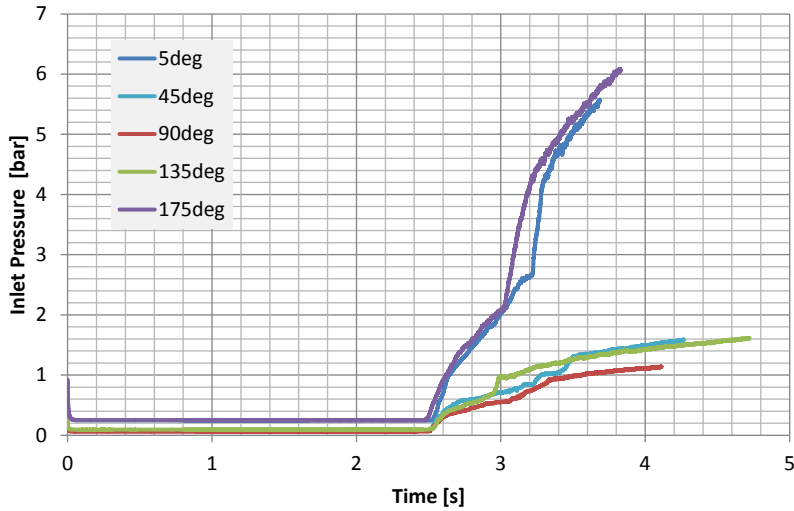


Figure 33: Inlet pressure for $h = 1 \text{ mm}$, $\theta = [5^\circ, 45^\circ, 90^\circ, 135^\circ, 175^\circ]$, $\rho_c = 1600 \text{ kg/m}^3$, and $\mu_c = 0.05 \text{ Pa}\cdot\text{s}$. Geometry: axis symmetric.

In Figure 34 we show the cement front position and pressure drop from inlet to outlet as function of time for a case with $\theta = 45^\circ$, $h = 1 \text{ mm}$. In this case we have used axis-symmetric geometry. The cement front position is here approximated by assuming plug flow, i.e. the front position is calculated from the cement volume in the fracture $r_{\text{cement}}^{\text{front}}(t) \approx R_{\text{joint}}^{\text{out}} \sqrt{V_{\text{joint}}^{\text{cement}}(t)/V_{\text{joint}}^{\text{tot}}}$.⁴

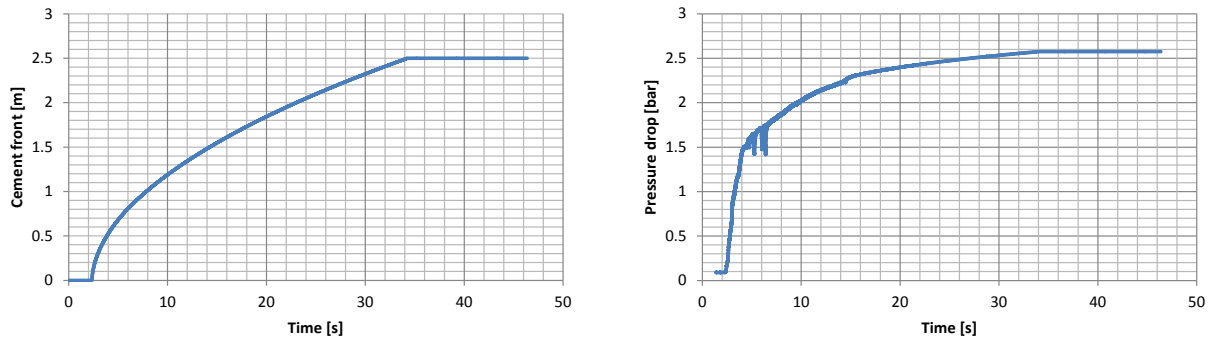


Figure 34: Cement front position and pressure drop for case with $\theta = 45^\circ$, $h = 1 \text{ mm}$. Geometry: axis symmetric.

⁴ Another possibility if the front is more smeared out could be to define the front position as the isoline where the cement volume fraction is e.g. 50%.

5.2.2 3D Axis symmetric - Non-Newtonian

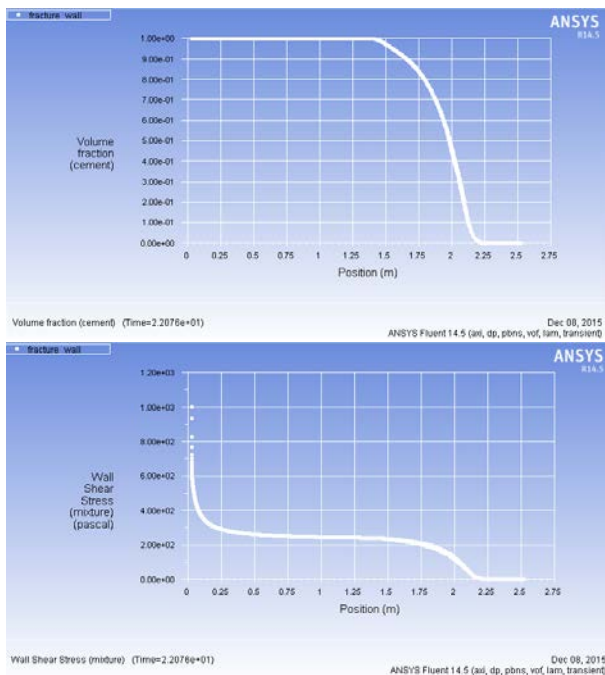
5.2.2.1 Yield stress effect

Here we study the replacement of water by cement in a simple axial symmetric joint, i.e. a disk with thickness h and a hole in the middle. We assume Bingham rheology for the cement with a yield stress: $\tau_0 = 200$ Pa, $K = 0.1$ Pa·s, $n = 1$. The yield stress is probably artificially high, but here we only want to demonstrate some phenomena.

The first case is a case with a pressure drop of $\Delta p = 10$ bar. Some radial profiles at $t \approx 22$ s from the centre of the joint and at the walls are shown in Figure 35. We observe that the volume fraction of cement shows a rather different shape at the two locations. This is also confirmed by the cross-sectional profiles taken at different radial distance in Figure 36a. Near the front we clearly see that the water forms a film at the walls and the cement flows in the middle. This water film will reduce the friction and reduce the effect of the yield stress.

The second case is a case with a pressure drop of $\Delta p = 5$ bar. Here we show the time development of the cement front position in Figure 37 together with the result from $\Delta p = 10$ bar. We clearly see that we reach a stagnation point and the front stops at about $r = 1.2$ m after about 35 s. This means that for this case the imposed pressure drop was too small to overcome the yield-stress for radial distances above approx. 1.2 m. Also here we see the same water film at the walls, see Figure 38.

Wall:



Center:

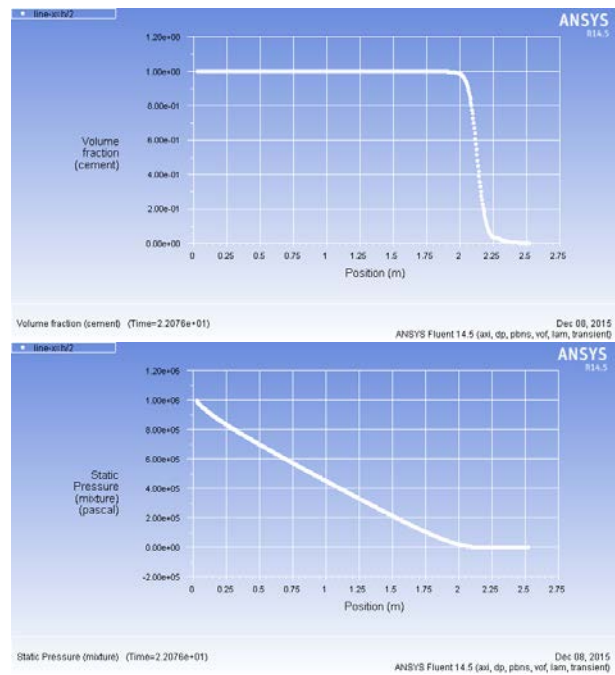


Figure 35: Radial variation of cement volume fraction, wall shear stress, and pressure ($h = 1$ mm, $\Delta p = 10$ bar, $\tau_0 = 200$ Pa, $K = 0.1$ Pa·s, $n = 1$). Geometry: Joint only, axis symmetric.

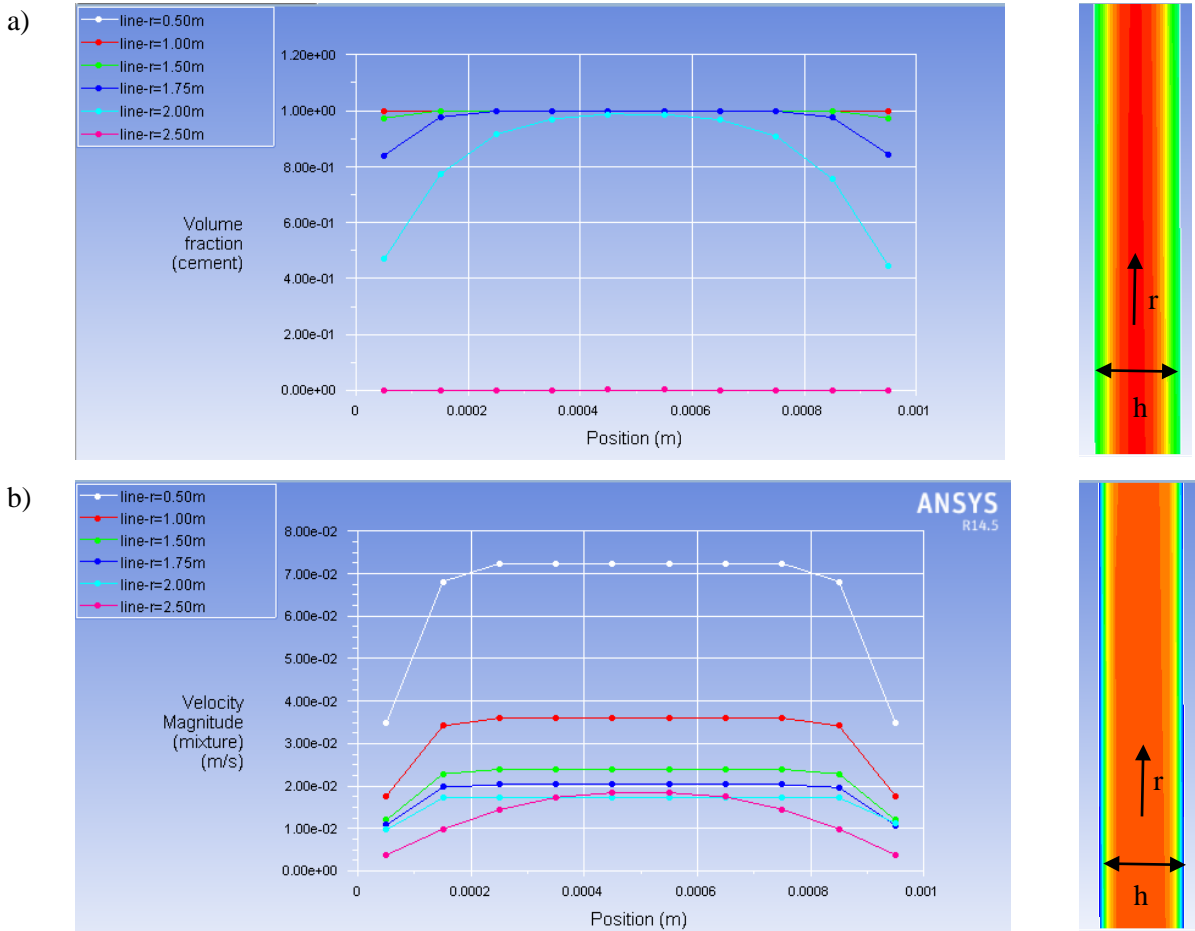


Figure 36: Profiles over the joint aperture at different radial distances at $t \approx 22\text{ s}$ for a) cement volume fraction and b) velocity magnitude ($h = 1\text{ mm}$, $\Delta p = 10\text{ bar}$, $\tau_0 = 200\text{ Pa}$, $K = 0.1\text{ Pa}\cdot\text{s}$, $n = 1$). The contour plots are taken at $r \approx 2.0\text{ m}$. Geometry: Joint only, axis symmetric.

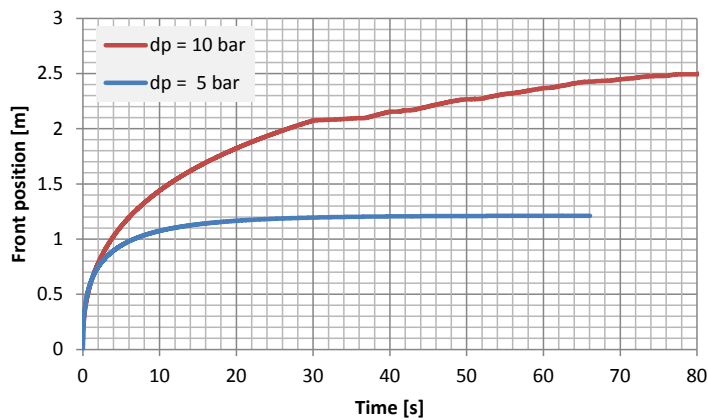


Figure 37: Cement front position as function of time ($h = 1\text{ mm}$, $\tau_0 = 200\text{ Pa}$, $K = 0.1\text{ Pa}\cdot\text{s}$, $n = 1$) for $\Delta p = 5\text{ bar}$ and 10 bar . Geometry: Joint only, axis symmetric.

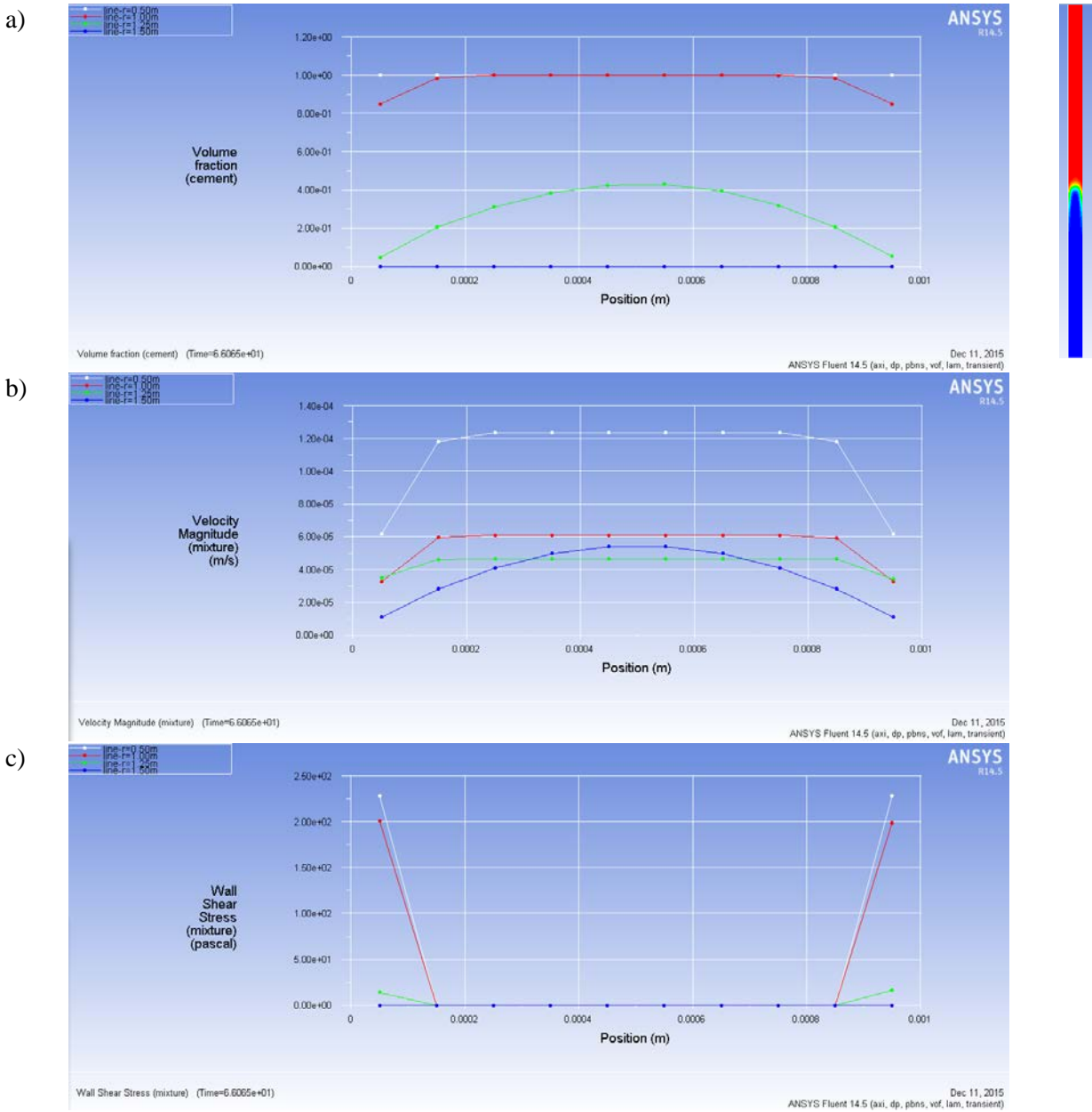


Figure 38: Profiles over the joint aperture at different radial distances for a) cement volume fraction, b) velocity magnitude, and c) wall shear stress ($h = 1 \text{ mm}$, $\Delta p = 5 \text{ bar}$, $\tau_0 = 200 \text{ Pa}$, $K = 0.1 \text{ Pa}\cdot\text{s}$, $n = 1$) at $t = 66 \text{ s}$. The aperture in the contour plot is increased by a factor 100 for visibility. Geometry: Joint only, axis symmetric.

6 SUMMARY

We have shown:

- Viscous effects dominate
- Joint orientation
 - Plays small role for cement spread forwards/backwards
 - Elliptic cross-section hole-joint increases effective joint inlet area. The effect is small (<10%) for $\theta > 30^\circ$.
- Simplified and or reduced models may be used
 - Axis-symmetric model (2D) with $\theta = 90^\circ$ - but would sacrifice some realism
 - Full 3D models of the joint only greatly simplify and reduce the computational cost of the flow simulations. A simplified pipe flow model can be used to prescribe the boundary conditions at each joint inlet. This allows more focus on the influence of aperture variations than for a full model of full 3D of both the borehole and joints.
- Water film (wetting) on the walls seem to play a role for cement injection
 - Specially important for cases with yield stress
 - Difficult to handle in simple analytical models, 3D simulations needed
- It is possible to develop a simulation workflow that can automate running statistical ensembles of joint sets. We believe that this is essential for any numerical work in this area since joint sets are inherently statistical and it is hard to assess the response without taking the statistics of the joint set into account during grouting.
- We believe the effect of grout pressure is strongly correlated to in-situ stress and joint jacking. The rationale is the strong dependence on joint aperture for flow and the fact that in situ stresses are close to equilibrium with in situ water prior to grouting for saturated rock. This can be further studied using local flow analysis.

7 FUTURE WORK

From our investigations we feel that flow analysis can safely be sectioned into two scales:

- Global flow analysis in a borehole and set of boreholes using statistical description of number of joints and extent of joints. This can be obtained using network models for flow analysis implemented in e.g. Matlab or as an Excel plugin. In such models one would use characteristic response correlations between pressure drop and flow as a function of joint parameters (roughness, aperture, converging/diverging aperture etc) and fluid properties (rheology). The resulting simulated system responses can be compared to volume-pressure curves from the injection equipment, and independent pressure readings in the grouting process.
- Local flow analysis in joints using statistical description of joint apertures and varying the flow parameters (flow rate, water-cement ratio, yield stress characteristics, particle size distributions). Such a detailed local model can be used to understand details of grout migration in joints, such as dependence on local topology of grout flow, particle segregation and bleeding effects, penetration distances and problems related to channelling and in-situ stresses (jacking). The local analysis will give output that can be used in the network model or as Excel tools. Local analysis would work well in collaboration with detailed grout flow experiments. The simulation tool of choice would be a commercial CFD package.

The two approaches are illustrated in the schematic below.

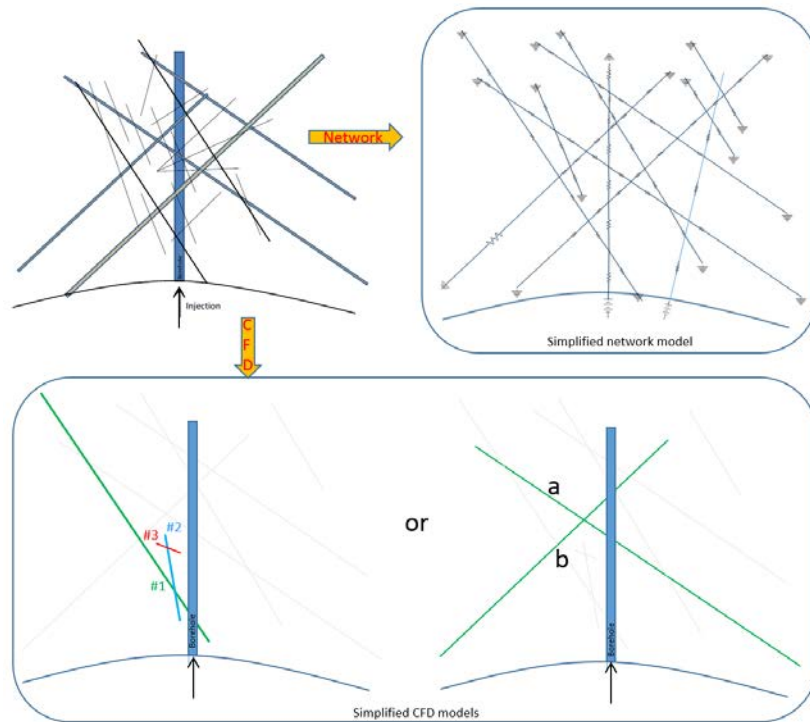


Figure 39: Conceptual models for modelling of grout flow in joint networks.

8 SYMBOL LIST

Symbol	Description	Unit
Latin:		
a_ε	Roughness amplitude	[m]
A	Area	[m ²]
D_b	Borehole diameter	[m]
f_ε	Roughness factor	[-]
h	Joint aperture	[m]
K	Consistency index in Herschel-Bulkley model	[Pa·s ⁿ]
n	Flow index in Herschel-Bulkley model	[-]
L	Length	[m]
m	Mass	[kg]
p	Pressure	[Pa]
Q	Volume flow rate	[m ³ /s]
R_b	Borehole radius	[m]
Re	Reynolds number ($Re = \rho UD / \mu$)	[-]
t	Time	[s]
U	Velocity	[m/s]
$U_{\text{joint}}^{\text{in}}$	Joint inlet velocity	[m/s]
\bar{U}	Cross-sectional averaged velocity	[m/s]
V	Volume	[m ³]
w	Width	[m]

X	Ratio: τ_0/τ_{wall}	[-]
Greek:		
δ	Distance into joint	[m]
Δp	Pressure drop	[Pa]
ΔL	Porous zone length	[m]
ε	Roughness	[m]
$\xi_{w/c}$	Water/cement ratio (mass ratio)	[-]
$\dot{\gamma}$	Strain rate	[1/s]
λ_ε	Roughness "wave length"	[m]
μ	Viscosity	[Pa·s]
μ_0	Viscosity limit in Herschel-Bulkley model	[Pa·s]
ρ	Density	[kg/m ³]
θ	Joint – Borehole angle	[°]
τ	Shear stress	[Pa]
τ_0	Yield stress	[Pa]
Subscripts:		
b	Borehole	
c	Cement	
geo	Geometric (geometric vs. effective aperture for porous zone)	
hole	Borehole	
in	Borehole inlet	
joint	Joint	
mix	Mixture	
w	Water	
wall	Wall	
0	Average joint aperture	
Superscripts:		

9 REFERENCES

1. Helene Strømsvik, Private communication
2. Cibich, W.: An Analytical Model for Enhanced Geothermal Systems (EGS), the University of Adelaide, SA (2008).
3. Mohammed, M.H., et al. (2014), Rheological Properties of Cement-Based Grouts Determined by Different Techniques. Engineering, 6, 217-229. <http://dx.doi.org/10.4236/eng.2014.65026>.
4. Chilton, R.A. and Stainsby, R., "Pressure loss equations for laminar and turbulent non-Newtonian pipe flow", J. Hydraulic Eng., 124:522-529, 1998.



Technology for a better society

www.sintef.no